

Implicit copula variational inference

Michael Stanley Smith and Rubén Loaiza-Maya

July 1, 2022

Michael Smith is Professor of Management (Econometrics) in the Melbourne Business School, University of Melbourne, Australia. Rubén Loaiza-Maya is Senior Lecturer in the Department of Econometrics and Business Statistics, Monash University, Australia. Correspondence should be directed to Michael Smith at mikes70au@gmail.com.

Acknowledgments: We thank Professor David Nott for discussions on the use of spherical co-ordinates. We also thank two referees, an Associate Editor and the Editor, Professor Galin Jones, for providing comments that improved the manuscript. We are grateful to Professor Mark Frank for placing his inequality data in the public domain.

Implicit copula variational inference

Abstract

Key to effective generic, or “black-box”, variational inference is the selection of an approximation to the target density that balances accuracy and speed. Copula models are promising options, but calibration of the approximation can be slow for some choices. Smith et al. (2020) suggest using tractable and scalable “implicit copula” models that are formed by element-wise transformation of the target parameters. We propose an adjustment to these transformations that make the approximation invariant to the scale and location of the target density. We also show how a sub-class of elliptical copulas have a generative representation that allows easy application of the re-parameterization trick and efficient first order optimization. We demonstrate the estimation methodology using two statistical models as examples. The first is a mixed effects logistic regression, and the second is a regularized correlation matrix. For the latter, standard Markov chain Monte Carlo estimation methods can be slow or difficult to implement, yet our proposed variational approach provides an effective and scalable estimator. We illustrate by estimating a regularized Gaussian copula model for income inequality in U.S. states between 1917 and 2018. An Online Appendix and MATLAB code to implement the method are available as Supplementary Materials.

Keywords: Elliptical copula; Factor model approximation; Re-parameterization trick; Spherical co-ordinates; Stochastic gradient ascent; Variational Bayes.

1 Introduction

Variational inference (VI) methods are increasingly used for the Bayesian estimation of big or complex statistical models. They require the selection of a variational approximation (VA) to the posterior distribution and an optimization approach for its calibration. Recent focus is on so-called “black box” VI methods (Ranganath et al., 2014) that combine generic VAs and optimization methods that require little or no tailoring to the statistical model being estimated. One promising black box approach is “copula VI” (Tran et al., 2015, Han et al., 2016, Smith et al., 2020, Gunawan et al., 2021), where copula models are used as generic VAs. Copula models are multivariate distributions constructed from marginals and a copula function; see Nelsen (2006) for an introduction. However, for many choices of copula function and/or marginals, the resulting VA can be computationally expensive to calibrate, limiting their adoption. To address this problem, Smith et al. (2020) show that “implicit copula” models can be flexible, scalable and fast to calibrate. The objective of this paper is to refine, extend and demonstrate the efficacy of their approach.

An implicit copula is constructed from a known continuous multivariate distribution $\boldsymbol{\psi} \sim F$ by inverting Sklar’s theorem; see Smith (2021). An attractive feature for VI is that implicit copula models can be represented as a one-to-one element-wise transformation between $\boldsymbol{\psi}$ and the model parameters $\boldsymbol{\theta}$ (also called “latent variables” in the machine learning literature). Smith et al. (2020) show that selecting tractable parametric forms for this transformation and the distributional family of F , allows ready application of the “re-parameterization trick”. This trick facilitates efficient implementation of stochastic gradient optimization algorithms for calibration of the implicit copula VA. We extend this idea here in three ways. First, the transformations suggested by these authors are shown to produce VAs that have a level of accuracy that varies with the location and scale of $\boldsymbol{\theta}$, which is a poor property. An adjustment to the transformations are proposed to correct for this. Second, for F we consider the sub-class of elliptical distributions that can be expressed as a scale mixture of normals. These have a generative representation that is amenable to the re-parameterization trick. Third, we follow Miller et al. (2017), Ong et al. (2018), Mishkin et al.

(2018) and others by adopting a sparse factor (also called a “low rank plus diagonal”) decomposition for the scale matrix Σ of distribution F . To identify the elliptical copula Σ should have a leading diagonal of ones, and we show how to use spherical co-ordinates to impose this bound. The end result is a class of elliptical copula model VAs that is scalable and fast to calibrate.

Other copula VI methods include that suggested by Tran et al. (2015) who use vine copulas. Calibration in high dimensions is typically slow compared to implicit copulas. Chi et al. (2021) suggest speeding up Monte Carlo gradient estimates in vine copula VI using draws under a mean field simplification. However, such estimates are more noisy than those computed using an effective re-parameterization gradient. The simplest implicit copula is the Gaussian copula, which was first employed as a VA by Han et al. (2016). Smith et al. (2020) extend this to the skew-normal copula and exploit sparse factorizations of the form in Ong et al. (2018) for the scale matrix and the re-parameterization trick. Gunawan et al. (2021) generalize the VI method of Smith et al. (2020) to a copula formed from a mixture of normals. Each mixture component is calibrated sequentially using a variational boosting algorithm, although the re-parameterization gradients can remain noisy in this case (Miller et al., 2017) and more computationally demanding estimates are necessary. The transformations suggested in our paper can also be used to make the VA of Gunawan et al. (2021) invariant to changes in the location and scale of θ . Hirt et al. (2019) propose a flexible VA that is motivated by (but is not) a copula model. As with our approach, their proposed VA has a generative representation that allows efficient implementation of stochastic gradient optimization.

To illustrate the increase in accuracy that our VA can provide compared to that in Smith et al. (2020), we re-examine their mixed logistic regression example. But our main application is the estimation of a regularized correlation matrix Ω , which is an important problem in statistical modeling (Rothman et al., 2008). Following Rebonato and Jäckel (1999) and others, we re-parameterize $\Omega = LL^\top$ using spherical co-ordinates for the Cholesky factor L . We then use a horseshoe prior (Carvalho et al., 2010) for a transformation of these angles that provides adaptive shrinkage of partial correlations towards zero. Estimation of the joint posterior of Ω and the shrinkage hyperparameters using standard MCMC methods can be prohibitively slow. However, implicit copula

VI can be employed to successfully estimate Ω in higher dimensions than MCMC. We show how to do so for a regularized Gaussian copula correlation matrix for annual income inequality in 49 U.S. states between 1917 and 2018. A rich pattern of interstate dependence that mirrors geographical and socio-economic commonalities between states is observed. A t-copula model VA is shown to capture the posterior more accurately than either a t-distribution or mean field approximations.

The rest of the paper is organized as follows. Section 2 gives a brief introduction to copula VI, with a focus on implicit copula VI. Section 3 details our extension and refinement of the methodology of Smith et al. (2020). Section 4 contains the two examples, while Section 5 concludes. Appendix A gives the closed form gradients required to implement the SGA algorithm. An Online Appendix provides further details on notation used, the derivatives, examples, and MATLAB code.

2 Copula variational inference

2.1 Variational inference

Consider a statistical model with continuous parameters $\boldsymbol{\theta} = (\theta_1, \dots, \theta_m)^\top$, data \mathbf{y} , and posterior density $p(\boldsymbol{\theta}|\mathbf{y}) \propto p(\mathbf{y}|\boldsymbol{\theta})p(\boldsymbol{\theta}) = g(\boldsymbol{\theta})$. Variational inference approximates $p(\boldsymbol{\theta}|\mathbf{y})$ with a density $q(\boldsymbol{\theta})$ that is called a “variational approximation” (VA). The approximation is obtained by minimizing a divergence measure between q and the posterior, with the Kullback-Leibler (KL) divergence the most common choice. In this case, the optimal approximating density in a family \mathcal{F} is $q^* = \operatorname{argmax}_{q \in \mathcal{F}} \mathcal{L}(q)$, where

$$\mathcal{L}(q) = \int \log \frac{g(\boldsymbol{\theta})}{q(\boldsymbol{\theta})} q(\boldsymbol{\theta}) d\boldsymbol{\theta} = E_q [\log g(\boldsymbol{\theta}) - \log q(\boldsymbol{\theta})]$$

is called the evidence lower bound (ELBO).

In many applications, the family \mathcal{F} is specific to the statistical model being estimated. However, generic fixed form approximations that can be employed to estimate a wide range of statistical models are also used. These have densities $q_\lambda(\boldsymbol{\theta})$ with variational parameters $\boldsymbol{\lambda}$ that fully specify the density, so that $q^*(\boldsymbol{\theta}) = q_{\boldsymbol{\lambda}^*}(\boldsymbol{\theta})$ with $\boldsymbol{\lambda}^* = \operatorname{argmax}_{\boldsymbol{\lambda}} \mathcal{L}(q_\lambda)$. When combined with generic

optimization algorithms, the approach is called “black box” VI (Ranganath et al., 2014). In this paper we refer to solving this optimization problem as “calibration” of the VA.

It is common to use stochastic gradient ascent (SGA) optimization, as we do here. In SGA, given an initial, value $\boldsymbol{\lambda}^{(0)}$, the variational parameters are updated recursively as

$$\boldsymbol{\lambda}^{(s+1)} = \boldsymbol{\lambda}^{(s)} + \boldsymbol{\delta}^{(s)} \circ \widehat{\nabla_{\boldsymbol{\lambda}} \mathcal{L}(q_{\boldsymbol{\lambda}})} \Big|_{\boldsymbol{\lambda}=\boldsymbol{\lambda}^{(s)}}, \quad s = 0, 1, 2, \dots$$

Here, $\boldsymbol{\delta}^{(s)}$ is a vector of adaptive step sizes, the operator “ \circ ” is the element-wise product, and $\widehat{\nabla_{\boldsymbol{\lambda}} \mathcal{L}(q_{\boldsymbol{\lambda}})}$ is an unbiased estimator of the gradient evaluated at $\boldsymbol{\lambda} = \boldsymbol{\lambda}^{(s)}$. A low variance gradient estimator is the main requirement of effective SGA, and the “re-parameterization trick” is a particularly effective means of obtaining one. Here, the model parameters are re-parameterized as $\boldsymbol{\theta} = h(\boldsymbol{\varepsilon}, \boldsymbol{\lambda}) \sim q_{\boldsymbol{\lambda}}$, where h is a deterministic function and $\boldsymbol{\varepsilon}$ is distributed with density $f_{\boldsymbol{\varepsilon}}$ that is invariant to $\boldsymbol{\lambda}$. Then the ELBO is $\mathcal{L}(q_{\boldsymbol{\lambda}}) = E_{f_{\boldsymbol{\varepsilon}}} [\log g(h(\boldsymbol{\varepsilon}, \boldsymbol{\lambda})) - \log q_{\boldsymbol{\lambda}}(h(\boldsymbol{\varepsilon}, \boldsymbol{\lambda}))]$ and its gradient is

$$\begin{aligned} \nabla_{\boldsymbol{\lambda}} \mathcal{L}(q_{\boldsymbol{\lambda}}) &= E_{f_{\boldsymbol{\varepsilon}}} [\nabla_{\boldsymbol{\lambda}} \log g(h(\boldsymbol{\varepsilon}, \boldsymbol{\lambda})) - \nabla_{\boldsymbol{\lambda}} \log q_{\boldsymbol{\lambda}}(h(\boldsymbol{\varepsilon}, \boldsymbol{\lambda}))] \\ &= E_{f_{\boldsymbol{\varepsilon}}} \left[\frac{\partial h(\boldsymbol{\varepsilon}, \boldsymbol{\lambda})}{\partial \boldsymbol{\lambda}}^{\top} (\nabla_{\boldsymbol{\theta}} \log g(\boldsymbol{\theta}) - \nabla_{\boldsymbol{\theta}} \log q_{\boldsymbol{\lambda}}(\boldsymbol{\theta})) \right], \end{aligned} \quad (1)$$

see Ong et al. (2018). (The notational conventions for derivatives used in this paper are outlined in Part A of the Online Appendix). Equation (1) is widely called a “re-parameterization gradient” and a low variance unbiased estimate of it is obtained by generating draws $\boldsymbol{\varepsilon} \sim f_{\boldsymbol{\varepsilon}}$, computing $\boldsymbol{\theta} = h(\boldsymbol{\varepsilon}, \boldsymbol{\lambda})$ and then evaluating the terms in the parentheses at these values. It is often the case that only a single draw of $\boldsymbol{\varepsilon}$ is sufficient to produce a low noise gradient estimator, as we do here. Thus, to use SGA with the re-parameterization trick requires selecting a VA with density $q_{\boldsymbol{\lambda}}$ that admits a re-parameterization $\{f_{\boldsymbol{\varepsilon}}, h\}$ from which generation and computation of (1) is fast.

2.2 Copula model variational approximations

Copula models are scalable and tractable representations of multivariate distributions and have been explored previously as VAs by Han et al. (2016), Tran et al. (2015), Smith et al. (2020),

Gunawan et al. (2021) and Chi et al. (2021). A copula model VA has density

$$q_{\lambda}(\boldsymbol{\theta}) = c(\mathbf{u}; \boldsymbol{\pi}) \prod_{i=1}^m q_{\lambda_i}(\theta_i), \quad (2)$$

where $\mathbf{u} = (u_1, \dots, u_m)^\top$, $q_{\lambda_i}(\theta_i)$ is the marginal density of θ_i that is selected arbitrarily, and $u_i = Q_{\lambda_i}(\theta_i) = \int_{-\infty}^{\theta_i} q_{\lambda_i}(s) ds$. The function $c(\mathbf{u}; \boldsymbol{\pi})$ is called the ‘‘copula density’’ and is a well-defined density function on the unit cube $[0, 1]^m$ with uniform marginals and parameters $\boldsymbol{\pi}$. Typically, the copula is selected from a list, with vine (Czado, 2019) or elliptical (Fang et al., 2002) copulas the most popular in high dimensions. Thus, a copula model VA is usually specified by choices for $q_{\lambda_1}, \dots, q_{\lambda_m}$ and $c(\cdot; \boldsymbol{\pi})$, with variational parameters $\boldsymbol{\lambda} = (\boldsymbol{\pi}^\top, \boldsymbol{\lambda}_1^\top, \dots, \boldsymbol{\lambda}_m^\top)^\top$.

However, two problems can arise when using copula models as high-dimensional VAs. First, an efficient re-parameterization $\{f_\epsilon, h\}$ may be difficult to identify. Second, the derivative $\nabla_{\boldsymbol{\theta}} \log q_{\lambda}(\boldsymbol{\theta})$ is required to evaluate the re-parameterization gradient at (1). By the chain rule,

$$\nabla_{\boldsymbol{\theta}} \log q_{\lambda}(\boldsymbol{\theta}) = \frac{\partial \mathbf{u}}{\partial \boldsymbol{\theta}}^\top \left(\frac{\partial}{\partial \mathbf{u}} \log c(\mathbf{u}; \boldsymbol{\pi}) \right)^\top + \left(\frac{\partial}{\partial \theta_1} \log q_{\lambda_1}(\theta_1), \dots, \frac{\partial}{\partial \theta_m} \log q_{\lambda_m}(\theta_m) \right)^\top,$$

where $\nabla_{\boldsymbol{\theta}} \log q_{\lambda}(\boldsymbol{\theta})$ is a column vector. Here, the term $\frac{\partial}{\partial \mathbf{u}} \log c(\mathbf{u}; \boldsymbol{\pi})$ may be prohibitively slow to compute; for example, Chi et al. (2021) note this problem for a vine copula. However, ‘‘implicit copulas’’ defined through transformation are one class of copulas that can avoid both problems, as now discussed.

2.3 Implicit copula model variational approximations

Consider a continuous random vector $\boldsymbol{\psi} = (\psi_1, \dots, \psi_m)^\top$ with known parametric distribution $F(\boldsymbol{\psi}; \boldsymbol{\pi})$, marginals $F_1(\psi_1; \boldsymbol{\pi}_1), \dots, F_m(\psi_m; \boldsymbol{\pi}_m)$, and parameters $\boldsymbol{\pi} = \cup_{i=1}^m \boldsymbol{\pi}_i$. Then the copula of this distribution is unique and has density

$$c(\mathbf{u}; \boldsymbol{\pi}) = \frac{p(\boldsymbol{\psi}; \boldsymbol{\pi})}{\prod_{i=1}^m p_i(\psi_i; \boldsymbol{\pi}_i)}, \quad (3)$$

where $p(\boldsymbol{\psi}; \boldsymbol{\pi}) = \frac{\partial}{\partial \boldsymbol{\psi}} F(\boldsymbol{\psi}; \boldsymbol{\pi})$, $p_i(\psi_i; \boldsymbol{\pi}_i) = \frac{d}{d\psi_i} F_i(\psi_i; \boldsymbol{\pi}_i)$, and $\psi_i = F_i^{-1}(u_i; \boldsymbol{\pi}_i)$. The copula parameters $\boldsymbol{\pi}$ are constrained to ensure they are identified in the copula density at (3), which is called an implicit copula. (Note that in Smith et al. (2020) the constrained values are denoted $\tilde{\boldsymbol{\pi}}$ to

distinguish them from the unconstrained values $\boldsymbol{\pi}$, although we do not do so here.) Different choices for $F(\boldsymbol{\psi}; \boldsymbol{\pi})$ produce different copula families. These include Gaussian copulas, t copulas, elliptical copulas, skew t copulas, factor copulas and copula processes; Smith (2021) provides an overview of the broad class of implicit copulas.

An implicit copula can also be defined through the element-wise transformations

$$\psi_i = F_i^{-1}(Q_{\lambda_i}(\theta_i); \boldsymbol{\pi}_i) \equiv k_i(\theta_i), \text{ for } i = 1, \dots, m.$$

These are strictly increasing functions because F_i and Q_{λ_i} are also. If $k'_i(\theta_i) = \frac{d}{d\theta_i} k_i(\theta_i)$, then by a change of variables the marginal density of the VA is simply

$$q_{\lambda_i}(\theta_i) = p_i(\psi_i; \boldsymbol{\pi}_i) k'_i(\theta_i). \quad (4)$$

Thus, from (2)–(4) the joint density of the implicit copula model VA is

$$\begin{aligned} q_{\lambda}(\boldsymbol{\theta}) &= c(\mathbf{u}; \boldsymbol{\pi}) \prod_{i=1}^m q_{\lambda_i}(\theta_i) = \frac{p(\boldsymbol{\psi}; \boldsymbol{\pi})}{\prod_{i=1}^m p_i(\psi_i; \boldsymbol{\pi}_i)} \prod_{i=1}^m p_i(\psi_i; \boldsymbol{\pi}_i) k'_i(\theta_i) \\ &= p(\boldsymbol{\psi}; \boldsymbol{\pi}) \prod_{i=1}^m k'_i(\theta_i). \end{aligned} \quad (5)$$

Computing the re-parameterization gradient using the expression at (5) can be much simpler than that at (2) because it avoids evaluation of the term $\frac{\partial}{\partial \mathbf{u}} \log c(\mathbf{u}; \boldsymbol{\pi})$. To see this, if $k''_i(\theta_i) = \frac{d^2}{d\theta_i^2} k_i(\theta)$, then the derivative

$$\nabla_{\boldsymbol{\theta}} \log q_{\lambda}(\boldsymbol{\theta}) = \frac{\partial \boldsymbol{\psi}}{\partial \boldsymbol{\theta}}^{\top} \left(\frac{\partial}{\partial \boldsymbol{\psi}} \log p(\boldsymbol{\psi}; \boldsymbol{\pi}) \right)^{\top} + \left(\frac{k''_1(\theta_1)}{k'_1(\theta_1)}, \dots, \frac{k''_m(\theta_m)}{k'_m(\theta_m)} \right)^{\top}, \quad (6)$$

where $\frac{\partial \boldsymbol{\psi}}{\partial \boldsymbol{\theta}} = \text{diag}(k'_1(\theta_1), \dots, k'_m(\theta_m))$ is a diagonal matrix. This expression, and thus the re-parameterization gradient, is fast to compute whenever k'_i , k''_i and $\frac{\partial}{\partial \boldsymbol{\psi}} \log p(\boldsymbol{\psi}; \boldsymbol{\pi})$ are also.

A copula model is usually defined from (2) by selecting the marginals $q_{\lambda_1}, \dots, q_{\lambda_m}$ and copula c . However, the transformation representation motivates another way to define an implicit copula model by selecting k_1, \dots, k_m and $p(\boldsymbol{\psi}; \boldsymbol{\pi})$ instead. These can be chosen so that (6) and the re-parameterization gradient at (1) are fast to compute in high dimensions. In particular, picking each transformation k_i directly avoids the need to evaluate either F_i or Q_{λ_i} , which can be slow or difficult. In principle, any tractable distribution can be adopted for $\boldsymbol{\psi}$, with Smith (2021) outlining

a wide range of choices and their respective implicit copulas. In the next section we detail how to implement variational inference with a sub-class of elliptical copulas, but discuss the potential of other choices in Section 5.

3 Learnable elliptical copula model VA

3.1 Definition

For each k_i we select a parametric monotonically increasing function denoted as $k_{\tilde{\gamma}_i}$ with parameter vector $\tilde{\gamma}_i$, so that $\boldsymbol{\lambda} = \{\boldsymbol{\pi}, \tilde{\gamma}_1, \dots, \tilde{\gamma}_m\}$. Smith et al. (2020) suggest using the Yeo-Johnson (YJ) and the inverse G-and-H (iGH) transformations for $k_{\tilde{\gamma}_i}$, because they are popular in data analysis as transformations from asymmetric to symmetric distributions. (The G-and-H transformation is from symmetry, which is why its inverse is used.) However, both transformations produce marginals $q_{\lambda_i}(\theta_i)$ that are not invariant to changes in location and scale, as demonstrated in Section 3.2. We therefore introduce location and scale parameters μ_i and σ_i directly for θ_i , so that

$$\psi_i = k_{\tilde{\gamma}_i}(\theta_i) = t_{\gamma_i} \left(\frac{\theta_i - \mu_i}{\sigma_i} \right), \quad (7)$$

where t_{γ_i} is either the YJ or iGH transformation, or compositions of the two. The transformation $k_{\tilde{\gamma}_i}$ has parameters $\tilde{\gamma}_i = (\gamma_i^\top, \mu_i, \sigma_i)^\top$ and is fast to implement within SGA methods.

An elliptical distribution is employed for $\boldsymbol{\psi}$, in which case (3) is the density of an elliptical copula studied by Fang et al. (2002). We consider the sub-class of elliptical distributions that can be written as a scale mixture of normals with generative representation

$$\boldsymbol{\psi} = \sqrt{W} \mathbf{X}, \quad (8)$$

where $\mathbf{X} \sim N_m(\mathbf{0}, \Sigma)$ and $W \sim F_W(\cdot; \boldsymbol{\omega})$ are independent. In Section 3.4 it is discussed how this representation can be used to implement efficiently the SGA algorithm with the reparameterization trick. The density of an elliptical distribution with location zero and scale matrix Σ is

$$p(\boldsymbol{\psi}; \boldsymbol{\pi}) = |\Sigma|^{-1/2} \tilde{g}_{m, \boldsymbol{\omega}} \left(\boldsymbol{\psi}^\top \Sigma^{-1} \boldsymbol{\psi} \right),$$

where $\tilde{g}_{m,\omega}(x) = \mathcal{K}_{m,\omega}g_\omega(x)$, the function $g_\omega : [0, \infty) \rightarrow (0, \infty)$ with parameters ω , $\boldsymbol{\pi} = (\omega^\top, \text{vech}(\Sigma)^\top)^\top$, and $\mathcal{K}_{m,\omega} = \Gamma(\frac{m}{2})/(\pi^{\frac{m}{2}} \int_0^\infty t^{\frac{m}{2}-1}g_\omega(t)dt)$ is a constant. We set the location to zero and Σ to be a correlation matrix to identify their values, which is necessary because μ_i, σ_i are introduced in the transformation at (7).

While all elliptical distributions are closed under marginalization (i.e. the marginal of an elliptical distribution is also an elliptical distribution), only a sub-class have marginals of the same parametric family, which is a property called “consistency” by Kano (1994). This author shows that elliptical distributions with the stochastic representation at (8) are consistent whenever the distribution of W is not a function of m . In this case the marginal has density $p_i(\psi_i; \boldsymbol{\pi}_i) = \tilde{g}_{1,\omega}(\psi_i^2)$ with $\boldsymbol{\pi}_i = \omega$, which can be used to define the implicit copula density at (3). Inconsistent elliptical distributions can also be used in our framework, where $\psi_i = \sqrt{W}X_i$ has density of a different parametric form. Table 1 gives four elliptical distributions that are scale mixtures of normals. They are the consistent Gaussian, t and Laplace distributions, and the inconsistent exponential power distribution. For each, the function $\tilde{g}_{m,\omega}$, its derivative, ω and the distribution of W are given. These are necessary to implement variational inference using their implicit copula models as VAs.

From (5) our proposed learnable VA has joint and marginal densities

$$q_\lambda(\boldsymbol{\theta}) = |\Sigma|^{-1/2} \tilde{g}_{m,\omega}(\boldsymbol{\psi}^\top \Sigma^{-1} \boldsymbol{\psi}) \prod_{i=1}^m t'_{\gamma_i} \left(\frac{\theta_i - \mu_i}{\sigma_i} \right) \frac{1}{\sigma_i}, \quad (9)$$

$$q_{\lambda_i}(\theta_i) = p_i(\psi_i; \boldsymbol{\pi}_i) t'_{\gamma_i} \left(\frac{\theta_i - \mu_i}{\sigma_i} \right) \frac{1}{\sigma_i}, \quad (10)$$

where $p_i(\psi_i; \boldsymbol{\pi}_i) = \tilde{g}_{1,\omega}(\psi_i^2)$ if the distribution for $\boldsymbol{\psi}$ is consistent. Notice that by introducing μ_i and σ_i , the marginal density for θ_i is flexible in terms of its location and scale. In contrast, Smith et al. (2020) and Gunawan et al. (2021) instead include a location and scale for ψ_i (and not for θ_i) which restricts the flexibility of the marginal approximation as illustrated in Section 3.2 below.

Table 1: Four Elliptical Distributions with Scale Mixture of Normals Generative Representations

Distribution	$\tilde{g}_{m,\omega}(x)$	$\tilde{g}'_{m,\omega}(x)$	ω	W Distribution or Density
Gaussian $\psi \sim N_m(\mathbf{0}, \Sigma)$	$(2\pi)^{-m/2} \exp\left(-\frac{x}{2}\right)$	$-\frac{1}{2}\tilde{g}_{m,\omega}(x)$	\emptyset	Point Mass at 1
Symmetric Laplace $\psi \sim SL_m(\mathbf{0}, \Sigma)$	$\frac{2}{(2\pi)^{m/2}} \left(\frac{x}{2}\right)^{\nu/2} K_\nu(\sqrt{2x})$ with $\nu = (2 - m)/2$	$c_1 \left[\left(\frac{x}{2}\right)^{\frac{\nu-1}{2}} K'_\nu(\sqrt{2x}) + \frac{\nu}{4} \left(\frac{x}{2}\right)^{\frac{\nu-2}{2}} K_\nu(\sqrt{2x}) \right]$	\emptyset	$W \sim \text{Exp}(1)$
Multivariate t $\psi \sim t_m(\mathbf{0}, \Sigma, \nu)$	$\frac{\Gamma(\frac{\nu+m}{2})}{\Gamma(\frac{\nu}{2})(\pi\nu)^{m/2}} \left(1 + \frac{x}{\nu}\right)^{-(\nu+m)/2}$	$-\frac{(\nu+m)}{2\nu} \left(1 + \frac{x}{\nu}\right)^{-1} \tilde{g}_{m,\omega}(x)$	$\nu > 0$	$W \sim \nu/\chi^2(\nu)$
Exponential Power $\psi \sim EP_m(\mathbf{0}, \Sigma, \beta)$	$\frac{m\Gamma(\frac{m}{2})}{\Gamma(1+\frac{m}{2\beta})\pi^{\frac{m}{2}} 2^{1+\frac{m}{2\beta}}} \exp\left(-\frac{1}{2}x^\beta\right)$	$-\frac{\beta}{2}x^{\beta-1}\tilde{g}_{m,\omega}(x)$	$0 < \beta \leq 1$	$f_W(w) = \frac{2^{1+\frac{m}{2}-\frac{m}{2\beta}}\Gamma(1+\frac{m}{2})}{\Gamma(1+\frac{m}{2\beta})} \times w^{m-3}f_{S,\beta}(w^{-2}; 2^{1-\frac{1}{\beta}})$

The distributions have density $p(\psi; \boldsymbol{\pi}) = |\Sigma|^{-1/2} \tilde{g}_{m,\omega}(\psi^\top \Sigma^{-1} \psi)$, where $\dim(\psi) = m$ and $\boldsymbol{\pi} = (\text{vech}(\Sigma)^\top, \omega^\top)^\top$, and stochastic representation as a scale mixture of normals. In the table, K_ν denotes the modified Bessel function of the third kind, Γ the gamma function, $\text{Exp}(1)$ an exponential distribution with parameter 1, $\chi^2(\nu)$ a chi-squared distribution with parameter ν , $f_{S,\alpha}(\cdot; \sigma)$ is the density of the positive stable distribution, and the constant $c_1 = \frac{2}{(2\pi)^{m/2}}$. For details on the Symmetric Laplace distribution see Kotz et al. (2001, Ch.5) and on the Exponential Power distribution see Gómez-Sánchez-Manzano et al. (2008).

3.2 Invariance of the marginal approximation

The marginal of the Gaussian copula model VA in Smith et al. (2020) has density

$$q_i^{\text{SLN2020}}(\theta_i) = \frac{1}{\sigma_{\psi_i}} \phi\left(\frac{\psi_i - \mu_{\psi_i}}{\sigma_{\psi_i}}\right) t'_{\gamma_i}(\theta_i),$$

where $\phi(x)$ is a $N(0, 1)$ density. The accuracy of this approximation varies with the location and scale of θ_i , which is a poor property for a VA. The same issue arises for other choices of $p(\boldsymbol{\psi}; \boldsymbol{\pi})$, including elliptical or mixture distributions. In contrast, the marginal approximation at (10) is invariant to the location and scale of θ_i by definition.

To demonstrate the impact on accuracy, we compare the ability of the marginal of q_i^{SLN2020} and the density at (10) with $p_i(\psi_i; \boldsymbol{\pi}_i) = \phi(\psi_i)$ to approximate the skew normal (SN) distribution of Azzalini and Dalla Valle (1996) for θ_i . Both VAs are constructed using the YJ transformation for t_{γ_i} . The SN parameters are set so that the Pearson skew coefficient is 0.8553, but the mean μ_{SN} and standard deviation σ_{SN} vary. Figure 1 plots the two optimal VAs (i.e. those with the minimum KL divergence) when (a) $\mu_{SN} = 15, \sigma_{SN} = 1$, and (b) $\mu_{SN} = 0, \sigma_{SN} = 1$. Simply changing the location μ_{SN} of the target distribution increases the KL divergence from 0.013 to 0.105 for q_i^{SLN2020} , but does not affect the accuracy of the approximation proposed here.

For the same case, Figure 2 plots the KL divergence of the two optimal VAs for a range of values of μ_{SN} and σ_{SN} . The accuracy of q_i^{SLN2020} varies substantially with μ_{SN} and σ_{SN} , and is much less accurate than that at (10) for most values of μ_{SN}, σ_{SN} . As an upper bound, the KL divergence for the optimal Gaussian approximation is also plotted as a horizontal line. This is nested by both VAs and it can be seen that q_i^{SLN2020} is only slightly more accurate than a Gaussian VA for some SN target distributions.

3.3 Factor correlation matrix

If Σ is unrestricted, then the number of elements increases quadratically with m , prohibiting usage of the VA in high dimensions. A popular solution for Gaussian VAs is to adopt a factor decomposition (also called a “low rank plus diagonal” decomposition in the machine learning literature) see Miller

et al. (2017), Ong et al. (2018), Mishkin et al. (2018) and Zhou et al. (2021) for recent examples. We follow this approach for the elliptical copula and set $\Sigma = BB^\top + D^2$, where $B = \{b_{i,j}\}$ is an $(m \times K)$ factor loading matrix, $D = \text{diag}(\mathbf{d})$ and $\mathbf{d} = (d_1, \dots, d_m)^\top$. To aid identification we set the upper triangle of B to zeros, and bound \mathbf{d} and the leading edge of B to be positive. Alternative identifying restrictions may also be used as discussed in Zhou et al. (2021) for Gaussian VAs. However, unlike in Smith et al. (2020), a complicating factor is that the positive definite matrix Σ has a leading diagonal of ones, so the constraints $d_j^2 + \sum_{k=1}^K b_{j,k}^2 = 1$, for $j = 1, \dots, m$ hold. A popular way of imposing such a constraint is to employ spherical co-ordinates; e.g. see Rebonato and Jäckel (1999). Here, this is equivalent to restricting $\mathbf{a}_j = (a_{j,1}, \dots, a_{j,K+1})^\top = (d_j, b_{j,1}, \dots, b_{j,K})^\top$ to lie on the surface of the $(K+1)$ -dimensional spherical space $\mathbb{S}^n = \{\mathbf{a}_j : \sum_{k=1}^{K+1} a_{j,k}^2 = 1\}$. We impose this spherical restriction by writing \mathbf{a}_j in terms of the angles $\boldsymbol{\varkappa}_j = (\varkappa_{j,1}, \dots, \varkappa_{j,K})^\top$, such that

$$a_{j,k} = \begin{cases} \cos \varkappa_{j,1} & \text{for } k = 1, \\ \cos \varkappa_{j,k} \prod_{i=1}^{k-1} \sin \varkappa_{j,i} & \text{for } 1 < k < K+1, \\ \prod_{i=1}^{K-1} \sin \varkappa_{j,i} & \text{for } k = K+1, \end{cases} \quad (11)$$

where $\varkappa_{j,k} \in (0, \pi)$ if $k < K$ and $\varkappa_{j,K} \in (0, 2\pi)$. There is a one-to-one relationship between the angles and (B, \mathbf{d}) .

One last complication is that our SGA optimization method is applicable to unconstrained variational parameters. To address this, the angles are expressed using a further monotonic transformation to the vectors $\boldsymbol{\tau}_j = (\tau_{j,1}, \dots, \tau_{j,K})^\top \in \mathbb{R}^K$, with elements $\tau_{j,k} = \Phi_1^{-1}(\varkappa_{j,k}/\pi)$ for $k < K$ and $\tau_{j,K} = \Phi_1^{-1}(\varkappa_{j,K}/2\pi)$. Finally, the complete variational parameter vector is $\boldsymbol{\lambda} = (\boldsymbol{\mu}^\top, \boldsymbol{\sigma}^\top, \boldsymbol{\gamma}^\top, \boldsymbol{\tau}^\top, \boldsymbol{\omega}^\top)^\top$, with $\boldsymbol{\mu} = (\mu_1, \dots, \mu_m)^\top$, $\boldsymbol{\tau} = (\boldsymbol{\tau}_1^\top, \dots, \boldsymbol{\tau}_m^\top)^\top$, $\boldsymbol{\sigma} = (\sigma_1, \dots, \sigma_m)^\top$, $\boldsymbol{\gamma} = (\boldsymbol{\gamma}_1^\top, \dots, \boldsymbol{\gamma}_m^\top)^\top$ and $\boldsymbol{\omega}$ is dependent on the choice of elliptical distribution (which is simply $\boldsymbol{\omega} = \emptyset$ for the Gaussian and Laplace distributions). Using this parameterization, the derivative at (6) is fast to compute analytically; see Appendix A.

3.4 Application of the re-parametrization trick

For our transformation-based implicit copula

$$\boldsymbol{\theta} = h(\boldsymbol{\varepsilon}, \boldsymbol{\lambda}) = (\mu_1 + \sigma_1 t_{\gamma_1}^{-1}(\psi_1), \dots, \mu_m + \sigma_m t_{\gamma_m}^{-1}(\psi_m))^{\top}. \quad (12)$$

To employ the re-parameterization trick, $p(\boldsymbol{\psi}; \boldsymbol{\pi})$ must have a generative representation based on a random vector $\boldsymbol{\varepsilon}$ that is unrelated to $\boldsymbol{\lambda}$. The scale mixture of normals at (8) provides this representation, as detailed in Algorithm 1.

Algorithm 1 (*Generating $\boldsymbol{\theta}$ from the elliptical copula model VA*)

1. Generate independently $\mathbf{z} \sim N_m(\mathbf{0}, I)$, $\boldsymbol{\epsilon} \sim N_m(\mathbf{0}, I)$, $u \sim \text{Uniform}(0, 1)$ and set $\boldsymbol{\varepsilon} = (\mathbf{z}^{\top}, \boldsymbol{\epsilon}^{\top}, u)^{\top}$
 2. Set $w = F_W^{-1}(u; \boldsymbol{\omega})$ where F_W^{-1} is the quantile function of W
 3. Set $\boldsymbol{\psi} = \sqrt{w}(B\mathbf{z} + D\boldsymbol{\epsilon})$
 4. Set $\boldsymbol{\theta} = h(\boldsymbol{\varepsilon}, \boldsymbol{\lambda})$
-

In this algorithm, Step 2 is unnecessary for the Gaussian distribution for $\boldsymbol{\psi}$, while for other elliptical distributions F_W^{-1} can be evaluated either analytically or numerically. Because W is a scalar, the computational burden of this step does not increase with the dimension m of the target distribution. All other steps are computationally inexpensive.

4 Examples

We use two examples to illustrate the improvement that adopting the VA at (9) can provide.

4.1 Example 1: mixed logistic regression

We re-estimate the mixed logistic regression example outlined in Smith et al. (2020). This employs a longitudinal dataset on 500 subjects over 7 years with 8 fixed effects (including an intercept) and one subject-based $N(0, \exp(2\zeta))$ random effect. The exact posterior can be computed using MCMC methods, so that the accuracy of any VA can be judged. The posterior of random effect values are typically skewed, which is the case for this example. There are 9 model parameters and 500 random effect values, so that a VA to the augmented posterior has $m = 509$.

We employ a t-copula model VA with density at (9) where $\psi \sim t_m(\mathbf{0}, \Sigma, \nu)$, $\tilde{g}_{m,\omega}$ is specified in Table 1, and the invariant transformation at (7) is used to form the implicit copula. The Gaussian copula model VA outlined in Smith et al. (2020) (labeled SLN2020) is used as a comparison. In both cases, we set $K = 5$ factors and considered three transformations for t_{γ_i} : YJ, iGH and a composition of two YJ transforms (Double-YJ). We also use a t distribution VA, which corresponds to assuming identity transformations $t_{\gamma_i}(\theta_i) = \theta_i$ for $i = 1, \dots, m$ at (7). When calibrating each of the three t-copula models and the t distribution using SGA, we found the variational parameter $\nu^* > 29$, which indicates that a Gaussian copula dependence structure is optimal here. Figure 3 plots the first three posterior moments of the VAs (vertical axes) against their true values (horizontal axes). All approximations identify the posterior means and standard deviations well, but SLN2020 does a poor job of estimating the posterior skew in panel (f) in comparison to our proposed VA in panel (c). To further visualize, Figure 4 plots the exact and variational marginal posteriors of three random effect values. The increased accuracy of the VA at (9) compared to SLN2020 is clear.

4.2 Example 2: regularized correlation matrix

We consider estimation of a Gaussian copula model for multivariate data (not to be confused with the copula model VA) with parameter correlation matrix Ω . In high dimensions either Ω or Ω^{-1} is often assumed to be sparse or patterned; e.g. see Oh and Patton (2017). However, in some applications this may be unreasonable, so that Ω is a full matrix and a regularized estimator is used. Below we suggest regularization of Ω based on a spherical coordinate parameterization, and then apply our VI approach for estimation. We note that the problem of estimating a regularized correlation matrix also arises in random effects (Danaher et al., 2020), multivariate probit (Zhang et al., 2021) and other statistical models.

4.2.1 The Statistical Model

Denote as $\mathbf{y}_i = (y_{i,1}, \dots, y_{i,r})^\top$ the i th observation of an r -dimensional vector of data, and $\mathbf{y} = (\mathbf{y}_1^\top, \dots, \mathbf{y}_N^\top)^\top$. The Gaussian copula model for this data has likelihood

$$p(\mathbf{y}|\boldsymbol{\theta}) = \frac{1}{|\Omega|^{N/2}} \prod_{i=1}^N \exp \left[-\frac{1}{2} \mathbf{x}_i^\top (\Omega^{-1} - I_r) \mathbf{x}_i \right] \prod_{j=1}^r g_j(y_{i,j}), \quad (13)$$

where $\mathbf{x}_i = (\Phi^{-1}(u_{i,1}), \dots, \Phi^{-1}(u_{i,r}))^\top$, $u_{i,j} = G_j(y_{i,j})$ and G_j, g_j denote the marginal distribution and density functions of $y_{i,j}$. We follow Pinheiro and Bates (1996), Rebonato and Jäckel (1999) and Yoshida (2018), and set $\Omega = LL^\top$, where $L = \{l_{i,j}\}$ is a lower triangular Cholesky factor with elements written in terms of spherical co-ordinates $\vartheta_{i,j}$ as

$$l_{i,j} = \begin{cases} 1 & \text{if } i = j = 1 \\ \sin(\vartheta_{i,i-1}) \prod_{s=1}^{i-2} \sin(\vartheta_{i,s}) & \text{if } i = j > 1 \\ \cos(\vartheta_{i,j}) \prod_{s=1}^{j-1} \sin(\vartheta_{i,s}) & \text{if } i > j \text{ and } i > 1 \\ 0 & \text{otherwise,} \end{cases}$$

where $\prod_{s=1}^0 \sin(\vartheta_{i,s}) \equiv 1$ and $\vartheta_{i,j} \in [0, \pi)$. Denote $\boldsymbol{\vartheta}_i = (\vartheta_{i,1}, \dots, \vartheta_{i,i-1})^\top$, then the angles $\boldsymbol{\vartheta} = (\boldsymbol{\vartheta}_1^\top, \dots, \boldsymbol{\vartheta}_r^\top)^\top$ provide a unique parameterization of Ω . If $(X_1, \dots, X_m)^\top \sim N(\mathbf{0}, \Omega)$, each angle is related to a partial correlation as

$$\cos \vartheta_{i,j} = \text{Corr}(X_i, X_j | X_1, \dots, X_{j-1}) \equiv \rho_{i,j|1:(j-1)}.$$

Each angle is transformed to the real line by setting $\eta_{i,j} = \Phi^{-1}(\frac{\vartheta_{i,j}}{\pi})$. Each partial correlation $\rho_{i,j|1:(j-1)} = 0$ iff $\eta_{i,j} = 0$, so that shrinkage of $\eta_{i,j}$ towards zero is equivalent to shrinking the partial correlation to zero, representing conditional independence between X_i and X_j .

The parameters are stacked into the vector $\boldsymbol{\eta} = (\boldsymbol{\eta}_2^\top, \dots, \boldsymbol{\eta}_r^\top)^\top \equiv (\eta_1, \eta_2, \dots, \eta_{r(r-1)/2})^\top$, with $\boldsymbol{\eta}_i = (\eta_{i,1}, \dots, \eta_{i,i-1})^\top$. The horseshoe prior (Carvalho et al., 2010) is used to provide adaptive shrinkage towards zero (i.e. regularization), where

$$\eta_s | \xi, \chi_s \sim N(0, \xi \chi_s), \quad \chi_s | \nu_s \sim \mathcal{G}^{-1} \left(\frac{1}{2}, \frac{1}{\nu_s} \right), \quad \xi | \kappa \sim \mathcal{G}^{-1} \left(\frac{1}{2}, \frac{1}{\kappa} \right), \quad \nu_1, \dots, \nu_{r(r-1)/2}, \kappa \sim \mathcal{G}^{-1} \left(\frac{1}{2}, 20 \right),$$

where $\mathcal{G}^{-1}(a, b)$ is an inverse gamma distribution with parameters a and b . The posterior densities

of parameters that are regularized using the horseshoe prior are funnel-shaped and difficult to approximate (Betancourt and Girolami, 2015, Ghosh et al., 2019). To address this, Ingraham and Marks (2017) suggest adopting the “non-centered” re-parameterization

$$\eta_s = \tau_s \sqrt{\xi \chi_s}, \text{ for } s = 1, \dots, r(r-1)/2,$$

which simplifies the geometry of the posterior. Here, $\chi^\top, \nu^\top, \xi, \kappa$ are all positive, so we further transform them to the real line using logarithmic transformations. With this, the model parameter vector $\boldsymbol{\theta} = (\tau^\top, \log \chi^\top, \log \xi, \log \nu^\top, \log \kappa)^\top$. The posterior $p(\boldsymbol{\theta}|\mathbf{y}) \propto p(\mathbf{y}|\boldsymbol{\theta})p(\boldsymbol{\theta}) = g(\boldsymbol{\theta})$ and its gradient $\nabla_{\boldsymbol{\theta}} \log g(\boldsymbol{\theta})$ are available in closed form and are given in Part C of the Online Appendix.

4.2.2 U.S. income inequality data

The copula model is used to model the dependence between changes in income inequality in U.S. states from 1916 to 2018. Inequality is measured using the annual Gini coefficient, where higher values indicate higher income inequality. Data for the study were sourced from Mark Frank’s webpage at www.shsu.edu/econ_mwf/inequality.html using an approach detailed in Frank (2009). Due to missing observations the states of Alaska and Hawaii were removed, while the District of Columbia (Washington D.C.) was included. Let $\text{GINI}_{t,j}$ denote the Gini coefficient in year t for state j , then we set $y_{t,j} = \text{GINI}_{t,j} - \text{GINI}_{t-1,j}$ and estimate G_j in each state using a kernel density estimate (KDE). These are non-Gaussian, so that a copula model is appropriate; see Figure A1 in the Online Appendix. The copula data $u_{t,j}$ are then computed, and posterior inference for Ω evaluated for the two cases below.

Low dimensional case: two U.S. states

The first estimation is for the $r = 2$ most populous states of California and Texas. Here, $(\theta_1, \dots, \theta_5)^\top = (\tau_1, \log \chi_1, \log \xi, \log \nu_1, \log \kappa)^\top$ and we consider this case because in a low-dimensional setting the posterior can be computed using MCMC methods, allowing comparison with our VA. Figure 5 plots the univariate marginals $p(\theta_i|\mathbf{y})$ and bivariate marginals $p(\theta_i, \theta_j|\mathbf{y})$ evaluated using MCMC.

The posteriors are unimodal, skewed and dependent—precisely the type of distribution that can be captured well using an elliptical copula model VA. Figure 6 plots the equivalent marginals of the t-copula model VA, with t_{γ_i} being Double-YJ transforms and $K = 5$ factors (i.e. B is 5×5). These are given by (10) and bivariate slices of (9). The VA captures key features of the posterior distribution well, including the location, skew and dependence. There is some mild under-estimation of the posterior variance, which is a common feature of fixed-form VAs that may be rectified using a post-estimation adjustment (Yu et al., 2021).

Higher dimensional case: 49 U.S. states

The second case is estimation for all $r = 49$ U.S. states, so that Ω has $49(48/2) = 1176$ unique elements and, when including the horseshoe hyper-parameters, θ has $m = 3530$ elements. Table 2 summarizes the results for 20 different t-copula model VAs with differing numbers of columns K for matrix B and transformations t_{γ_i} employed. When the identity transformation $t_{\gamma_i}(\theta_i) = \theta_i$ is used, the VA is simply a t-distribution with a factor covariance matrix. When $K = 0$ the scale matrix Σ is diagonal and the VA is a mean field approximation over each element of θ .

The number of variational parameters $|\lambda|$ and the time taken to complete 1,000 steps of the SGA algorithm are reported. We found 15,000 steps is sufficient to calibrate each VA; for example, calibration took two hours for the t-copula model with $K = 15$ and the YJ transformation for t_{γ_i} using a low end desktop. Also reported is the median lower bound over the last 500 steps, labeled as $\overline{\text{LB}}$, with higher values indicating more accurate calibration. By this measure the copula model VAs are all much more accurate than a t-distribution, with the most accurate being the t-copula model with $K = 10, 15$ or 20 and the YJ transformation for t_{γ_i} .

Pairwise dependence in the fitted Gaussian copula can be measured by the matrix of Spearman correlations $\Omega^s = \frac{6}{\pi} \arcsin(\frac{1}{2}\Omega)$, where \arcsin is applied element-wise to $\frac{1}{2}\Omega$. Figure A2 (see Online Appendix) plots the point estimate of Ω^s from the optimal t-copula model VA to the posterior. To further visualize the results, we select the five contiguous western states of AZ, CA, NV, OR and WA, and then plot the variational posteriors of the pairwise Spearman correlations for these

Table 2: Summary of 20 VAs to the Posterior of the Gaussian Copula Model for U.S. Inequality

t_{γ_i}	Number of Columns in B				
	$K = 0$	$K = 5$	$K = 10$	$K = 15$	$K = 20$
	<i>Number of Variational Parameters λ</i>				
Identity	7,061	24,711	42,361	60,011	77,661
iGH	14,121	31,771	49,421	67,071	84,721
YJ	10,591	28,241	45,891	63,541	81,191
Double YJ	14,121	31,771	49,421	67,701	84,721
	<i>Time (Mins. per 1000 Steps)</i>				
Identity	5.6	5.9	6.4	8.3	13.1
iGH	5.6	6.1	6.6	8.8	13.7
YJ	5.6	5.9	6.4	8.3	13.2
Double YJ	5.5	5.9	6.5	8.4	13.2
	\overline{LB}				
Identity	416.6	466.3	534.8	521.2	530.9
iGH	596.7	480.4	657.5	565.0	610.4
YJ	650.0	657.1	664.8	663.8	668.9
Double YJ	637.5	640.5	648.8	649.3	655.3

The computation was implemented in serial using MATLAB on a low end DELL desktop with an Intel i7-10700 CPU @ 2.9Ghz.

states in Figure 7. This is undertaken for both the mean field t-distribution and the t-copula model VA with $K = 15$ and the YJ transformation. The impact of employing the more flexible VA can be seen; for example, the variational posterior for the correlation between WA and AZ is located at a lower value.

5 Discussion

This paper aims to refine and extend the copula VI approach outlined in Smith et al. (2020), making five contributions. First, Section 2 clarifies why implicit copula models are an attractive choice of VA in high dimensions, compared to other copula models such as vine copula models. Second, an adjustment to the transformations that define the implicit copula is proposed that increases the accuracy of the VA. Third, it is shown how to implement the re-parameterization trick for a sub-class of elliptical copulas. This is useful in practice because employing the re-parameterization gradient at (1) increases the efficiency of SGA greatly. Fourth, it is shown how spherical co-

ordinates can be used to represent the factor decomposition of Σ , and constrain it to a correlation matrix efficiently. Last, it is demonstrated how the proposed copula VI method can be used to approximate the complex posterior of a regularized correlation matrix. This is a difficult posterior to evaluate exactly in high dimensions using standard MCMC methods.

Elliptical copula VI is an attractive black box method for posteriors that are unimodal, have positive and negative dependencies between parameters, and exhibit high levels of skew, as in Figures 5 and 6. Gunawan et al. (2021) also employ implicit copula VI, but with a mixture of normals for $\psi \sim F$. This further extends the dependence structure of the VA, although calibration is more computationally demanding because the re-parameterization trick cannot be used directly. Compositions of parametric transformations can be considered at (7), although experiments (unreported) suggest little improvement in the accuracy of the VA. However, a promising direction for future work is to consider multivariate transformations of the implicit copula model to further enrich the VA, such as the sparse Householder transformations discussed by Hirt et al. (2019) and references therein; although, the resulting VA will no longer be a copula model with a known dependence structure. Another direction is to consider a Gaussian or other process for $\psi \sim F$. The resulting implicit copula is a “copula process” (Wilson and Ghahramani, 2010) which can admit a more complex dependence structure for the VA, while still exploiting the computational advantages outlined here. Finally, while we did not employ our method to estimate a Bayesian neural network, it can clearly be used to do so. For example, it would be interesting to consider the Bayesian neural network in Hirt et al. (2019), which uses the same horseshoe prior based regularization as is employed in our correlation matrix example.

Appendix A Gradients for implementation of SGA

This appendix provides the gradients to implement SGA with the re-parameterization trick for the proposed elliptical copula model VA at (9). They do not vary by choice of target density, and MATLAB code for their fast evaluation is provided in the Supplementary Material.

Expression for $\nabla_{\theta} \log q_{\lambda}(\boldsymbol{\theta})$

For the elliptical copula model VA, the gradient at (6) is

$$\nabla_{\theta} \log q_{\lambda}(\boldsymbol{\theta}) = \frac{g'_{m,\omega}(\boldsymbol{\psi}^{\top} \Sigma^{-1} \boldsymbol{\psi})}{g_{m,\omega}(\boldsymbol{\psi}^{\top} \Sigma^{-1} \boldsymbol{\psi})} 2 \frac{\partial \boldsymbol{\psi}}{\partial \boldsymbol{\theta}} \Sigma^{-1} \boldsymbol{\psi} + \left(\frac{t''_{\gamma_1} \left(\frac{\theta_1 - \mu_1}{\sigma_1} \right)}{t'_{\gamma_1} \left(\frac{\theta_1 - \mu_1}{\sigma_1} \right) \sigma_1}, \dots, \frac{t''_{\gamma_m} \left(\frac{\theta_m - \mu_m}{\sigma_m} \right)}{t'_{\gamma_m} \left(\frac{\theta_m - \mu_m}{\sigma_m} \right) \sigma_m} \right)^{\top},$$

with

$$\frac{\partial \boldsymbol{\psi}}{\partial \boldsymbol{\theta}} = \text{diag} \left(t'_{\gamma_1} \left(\frac{\theta_1 - \mu_1}{\sigma_1} \right) / \sigma_1, \dots, t'_{\gamma_m} \left(\frac{\theta_m - \mu_m}{\sigma_m} \right) / \sigma_m \right).$$

Expressions for t'_{γ_j} and t''_{γ_j} are provided in Table 1 of Smith et al. (2020) for both the YJ and iGH transformations, which are very fast to compute. The derivatives of compositions of these two transformations are also easily computed using a trivial application of the chain rule. Expressions for $g_{m,\omega}$ and $g'_{m,\omega}$ are given in Table 1 of this paper for the four elliptical copulas. For the Gaussian copula the first ratio simplifies to $\frac{g'_{m,\omega}(\boldsymbol{\psi}^{\top} \Sigma^{-1} \boldsymbol{\psi})}{g_{m,\omega}(\boldsymbol{\psi}^{\top} \Sigma^{-1} \boldsymbol{\psi})} = -1/2$, while for the t copula it simplifies to $\frac{g'_{m,\omega}(\boldsymbol{\psi}^{\top} \Sigma^{-1} \boldsymbol{\psi})}{g_{m,\omega}(\boldsymbol{\psi}^{\top} \Sigma^{-1} \boldsymbol{\psi})} = -\frac{v+m}{2\nu} \left[1 + \left(\frac{\boldsymbol{\psi}^{\top} \Sigma^{-1} \boldsymbol{\psi}}{\nu} \right) \right]^{-1}$.

Expression for $\frac{\partial \boldsymbol{\theta}}{\partial \boldsymbol{\lambda}} = \frac{\partial h(\boldsymbol{\varepsilon}, \boldsymbol{\lambda})}{\partial \boldsymbol{\lambda}}$

Denote $A = [\mathbf{d} \ B]$ to be the matrix of elements $a_{j,k}$, $\boldsymbol{\kappa} = (\boldsymbol{\kappa}_1^{\top}, \dots, \boldsymbol{\kappa}_m^{\top})^{\top}$, $P_1 = [\mathbf{0}_{K \times 1} \ I_K]^{\top}$ and $P_2 = (1, \mathbf{0}_{1 \times K})^{\top}$. The derivatives of $\boldsymbol{\theta} = h(\boldsymbol{\varepsilon}, \boldsymbol{\lambda})$ with respect to $\boldsymbol{\lambda} = (\boldsymbol{\mu}^{\top}, \boldsymbol{\sigma}^{\top}, \boldsymbol{\gamma}^{\top}, \boldsymbol{\tau}^{\top}, \boldsymbol{\omega}^{\top})^{\top}$ are

$$\begin{aligned} \frac{\partial \boldsymbol{\theta}}{\partial \boldsymbol{\mu}} &= I_m, & \frac{\partial \boldsymbol{\theta}}{\partial \boldsymbol{\sigma}} &= \text{diag} (t_{\gamma_1}^{-1}(\psi_1), \dots, t_{\gamma_m}^{-1}(\psi_m)), \\ \frac{\partial \boldsymbol{\theta}}{\partial \boldsymbol{\gamma}} &= \text{diag} \left(\sigma_1 \frac{\partial t_{\gamma_1}^{-1}(\psi_1)}{\partial \gamma_1}, \dots, \sigma_m \frac{\partial t_{\gamma_m}^{-1}(\psi_m)}{\partial \gamma_m} \right), \\ \frac{\partial \boldsymbol{\theta}}{\partial \boldsymbol{\tau}} &= \frac{\partial \boldsymbol{\theta}}{\partial \boldsymbol{\psi}} \frac{\partial \boldsymbol{\psi}}{\partial \boldsymbol{\kappa}} \frac{\partial \boldsymbol{\kappa}}{\partial \boldsymbol{\tau}}, & \frac{\partial \boldsymbol{\theta}}{\partial \boldsymbol{\omega}} &= \frac{\partial \boldsymbol{\theta}}{\partial \boldsymbol{\psi}} \frac{\partial \boldsymbol{\psi}}{\partial \boldsymbol{\omega}}, \end{aligned}$$

where

$$\frac{\partial \boldsymbol{\theta}}{\partial \boldsymbol{\psi}} = \text{diag} \left(\sigma_1 \frac{\partial t_{\gamma_1}^{-1}(\psi_1)}{\partial \psi_1}, \dots, \sigma_m \frac{\partial t_{\gamma_m}^{-1}(\psi_m)}{\partial \psi_m} \right), \text{ and } \frac{\partial \boldsymbol{\kappa}}{\partial \boldsymbol{\tau}} = \text{blockdiag} \left(\frac{\partial \boldsymbol{\kappa}_1}{\partial \boldsymbol{\tau}_1}, \dots, \frac{\partial \boldsymbol{\kappa}_m}{\partial \boldsymbol{\tau}_m} \right),$$

with $\frac{\partial \boldsymbol{\kappa}_j}{\partial \boldsymbol{\tau}_j} = \text{diag} (\phi(\tau_{j,1})\pi, \dots, \phi(\tau_{j,K-1})\pi, \phi(\tau_{j,K})2\pi)$, and

$$\frac{\partial \boldsymbol{\psi}}{\partial \boldsymbol{\kappa}} = \sqrt{w} \left[(\mathbf{z}^{\top} P_1^{\top}) \otimes I_m + \text{diag}(\boldsymbol{\epsilon}) (P_2^{\top} \otimes I_m) \right] K_{K+1,m} \frac{\partial A^{\top}}{\partial \boldsymbol{\kappa}},$$

with $\frac{\partial A^\top}{\partial \boldsymbol{\kappa}} = \text{blockdiag} \left(\frac{\partial \mathbf{a}_1}{\partial \boldsymbol{\kappa}_1}, \dots, \frac{\partial \mathbf{a}_m}{\partial \boldsymbol{\kappa}_m} \right)$ and

$$\left\{ \frac{\partial \mathbf{a}_i}{\partial \boldsymbol{\kappa}_i} \right\}_{j,l} = \begin{cases} \cos(\boldsymbol{\kappa}_{i,j}) \cos(\boldsymbol{\kappa}_{i,l}) \prod_{s \in \{1, \dots, j-1\} \setminus l} \sin(\boldsymbol{\kappa}_{i,s}) & \text{If } l < j \text{ and } j < K+1 \\ - \prod_{s=1}^j \sin(\boldsymbol{\kappa}_{i,s}) & \text{If } l = j \text{ and } j < K+1 \\ \cos(\boldsymbol{\kappa}_{i,l}) \prod_{s \in \{1, \dots, j-1\} \setminus l} \sin(\boldsymbol{\kappa}_{i,s}) & \text{If } l < j \text{ and } j = K+1 \\ 0 & \text{otherwise} \end{cases}.$$

Here, $K_{K+1,m}$ denotes the relevant commutation matrix. For details on the derivation of these expressions see Part B of the Online Appendix. The terms $\frac{\partial t_{\gamma_j}^{-1}(\cdot)}{\partial \gamma_j}$ and $\frac{\partial t_{\gamma_j}^{-1}(\cdot)}{\partial \psi_j}$ are provided in Table 1 of Smith et al. (2020) for both the YJ and iGH transformations.

For the Gaussian and Laplace distributions it is unnecessary to evaluate the derivative $\frac{\partial \boldsymbol{\psi}}{\partial \boldsymbol{\omega}}$ because $\boldsymbol{\omega} = \emptyset$. However, in general $\boldsymbol{\psi} = \sqrt{w}(B\mathbf{z} + D\boldsymbol{\epsilon})$ with $w = F_W^{-1}(u; \boldsymbol{\omega})$, so that

$$\frac{\partial \boldsymbol{\psi}}{\partial \boldsymbol{\omega}} = (B\mathbf{z} + D\boldsymbol{\epsilon}) \times \left\{ \frac{1}{2(F_W^{-1}(u; \boldsymbol{\omega}))^{1/2}} \left(\frac{\partial}{\partial \boldsymbol{\omega}} F_W^{-1}(u; \boldsymbol{\omega}) \right) \right\}$$

For the t distribution $\boldsymbol{\omega} = \nu$, $F_W^{-1}(u; \boldsymbol{\omega}) = \nu / F_X^{-1}(1 - u; \nu)$ with F_X the distribution function of $X \sim \chi^2(\nu)$, and $\frac{\partial}{\partial \boldsymbol{\omega}} F_W^{-1}(u; \boldsymbol{\omega})$ is computed numerically.

Supplementary Materials

Online Appendix: provides further details on notation used, the derivatives, examples and MATLAB code.

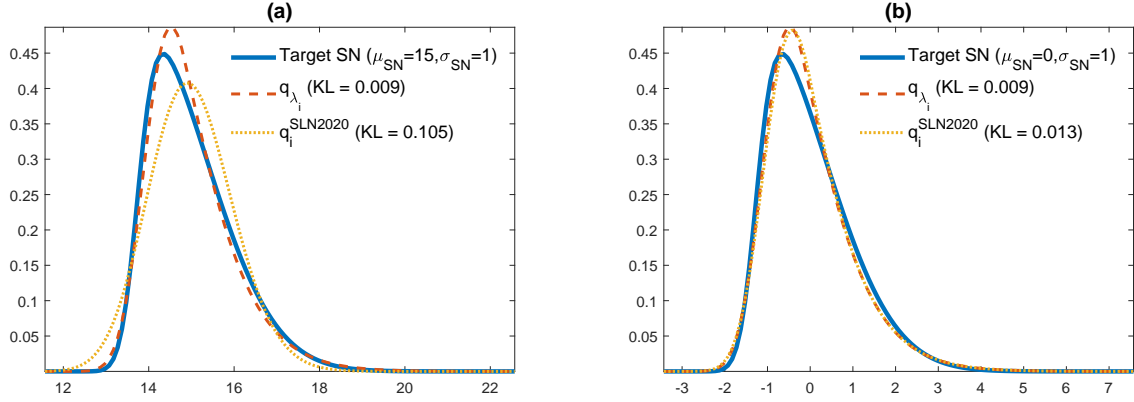
Code and Data Zip File: provides MATLAB code and data to replicate our results, and apply the method to other datasets and/or models.

References

- Azzalini, A. and Dalla Valle, A. (1996). The multivariate skew-normal distribution. *Biometrika*, 83(4):715–726.
- Betancourt, M. and Girolami, M. (2015). Hamiltonian Monte Carlo for hierarchical models. *Current trends in Bayesian methodology with applications*, 79(30):2–4.
- Carvalho, C. M., Polson, N. G., and Scott, J. G. (2010). The horseshoe estimator for sparse signals. *Biometrika*, 97(2):465–480.
- Chi, J., Ouyang, J., Zhang, A., Wang, X., and Li, X. (2021). Fast copula variational inference. *Journal of Experimental & Theoretical Artificial Intelligence*, 0(0):1–16.
- Czado, C. (2019). Analyzing dependent data with vine copulas. *Lecture Notes in Statistics*, Springer.
- Danaher, P. J., Danaher, T. S., Smith, M. S., and Loaiza-Maya, R. (2020). Advertising effectiveness for multiple retailer-brands in a multimedia and multichannel environment. *Journal of Marketing Research*, 57(3):445–467.
- Fang, H.-B., Fang, K.-T., and Kotz, S. (2002). The meta-elliptical distributions with given marginals. *Journal of Multivariate Analysis*, 82(1):1–16.
- Frank, M. W. (2009). Inequality and growth in the united states: Evidence from a new state-level panel of income inequality measures. *Economic Inquiry*, 47(1):55–68.
- Ghosh, S., Yao, J., and Doshi-Velez, F. (2019). Model selection in Bayesian neural networks via horseshoe priors. *Journal of Machine Learning Research*, 20(182):1–46.
- Gómez-Sánchez-Manzano, E., Gómez-Villegas, M., and Marín, J. (2008). Multivariate exponential power distributions as mixtures of normal distributions with bayesian applications. *Communications in Statistics—Theory and Methods*, 37(6):972–985.
- Gunawan, D., Kohn, R., and Nott, D. (2021). Flexible variational Bayes based on a copula of a mixture of normals. *arXiv preprint arXiv:2106.14392*.
- Han, S., Liao, X., Dunson, D. B., and Carin, L. C. (2016). Variational Gaussian copula inference. In Gretton, A. and Robert, C. C., editors, *Proceedings of the 19th International Conference on Artificial Intelligence and Statistics*, volume 51, pages 829–838, Cadiz, Spain. JMLR Workshop and Conference Proceedings.
- Hirt, M., Dellaportas, P., and Durmus, A. (2019). Copula-like variational inference. In Wallach, H., Larochelle, H., Beygelzimer, A., d'Alché-Buc, F., Fox, E., and Garnett, R., editors, *Advances in Neural Information Processing Systems*, volume 32.
- Ingraham, J. and Marks, D. (2017). Variational inference for sparse and undirected models. In *International Conference on Machine Learning*, pages 1607–1616. PMLR.
- Kano, Y. (1994). Consistency property of elliptic probability density functions. *Journal of Multivariate Analysis*, (1):139–147.
- Kotz, S., Kozubowski, T. J., and Podgórski, K. (2001). *The Laplace Distribution and Generalizations*. Springer.

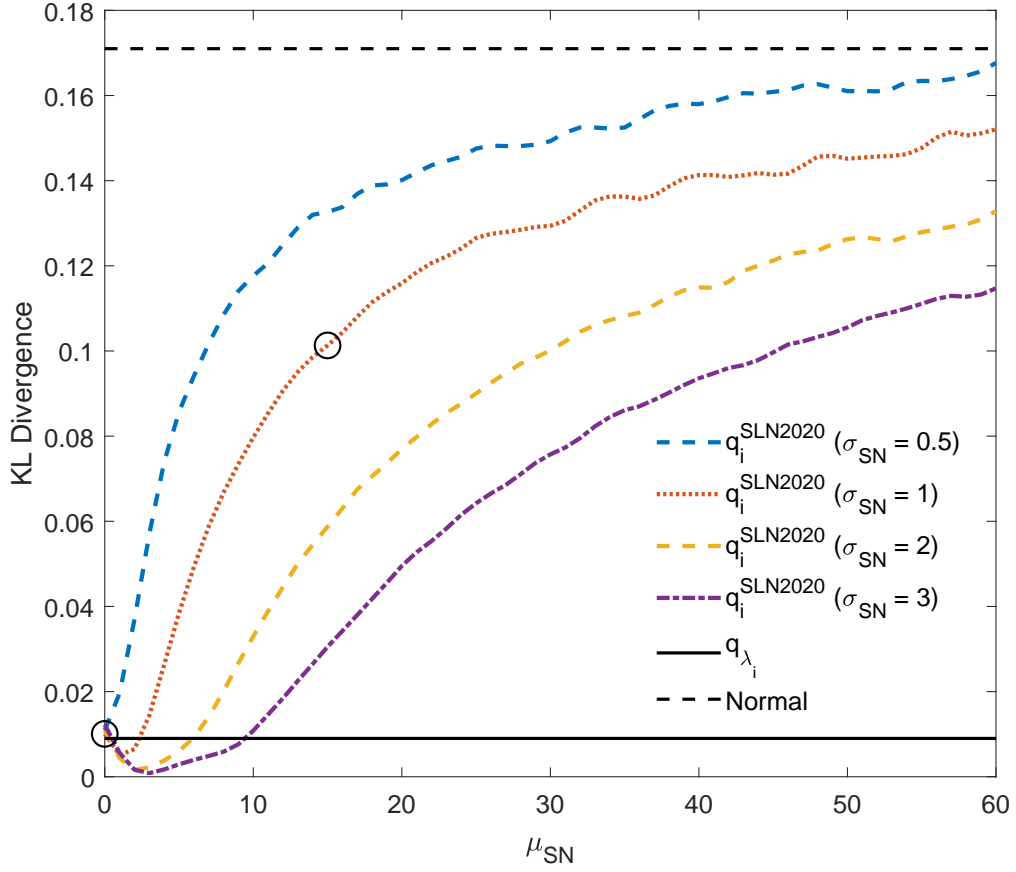
- Miller, A. C., Foti, N. J., and Adams, R. P. (2017). Variational boosting: Iteratively refining posterior approximations. In *International Conference on Machine Learning*, pages 2420–2429. PMLR.
- Mishkin, A., Kunstner, F., Nielsen, D., Schmidt, M., and Khan, M. E. (2018). Slang: Fast structured covariance approximations for Bayesian deep learning with natural gradient. *arXiv preprint arXiv:1811.04504*.
- Nelsen, R. B. (2006). *An Introduction to Copulas*. Springer-Verlag, New York, Secaucus, NJ, USA.
- Oh, D. H. and Patton, A. J. (2017). Modeling dependence in high dimensions with factor copulas. *Journal of Business & Economic Statistics*, 35(1):139–154.
- Ong, V. M.-H., Nott, D. J., and Smith, M. S. (2018). Gaussian variational approximation with factor covariance structure. *Journal of Computational and Graphical Statistics*, 27(3):465–478.
- Pinheiro, J. C. and Bates, D. M. (1996). Unconstrained parametrizations for variance-covariance matrices. *Statistics and computing*, 6(3):289–296.
- Ranganath, R., Gerrish, S., and Blei, D. (2014). Black Box Variational Inference. In Kaski, S. and Corander, J., editors, *Proceedings of the Seventeenth International Conference on Artificial Intelligence and Statistics*, volume 33 of *Proceedings of Machine Learning Research*, pages 814–822, Reykjavik, Iceland. PMLR.
- Rebonato, R. and Jäckel, P. (1999). The most general methodology to create a valid correlation matrix for risk management and option pricing purposes. *Journal of Risk*, 2(2):17–27.
- Rothman, A. J., Bickel, P. J., Levina, E., and Zhu, J. (2008). Sparse permutation invariant covariance estimation. *Electronic Journal of Statistics*, 2:494 – 515.
- Smith, M. S. (2021). Implicit copulas: An overview. *Econometrics and Statistics*, Forthcoming.
- Smith, M. S., Loaiza-Maya, R., and Nott, D. J. (2020). High-dimensional copula variational approximation through transformation. *Journal of Computational and Graphical Statistics*, 29(4):729–743.
- Tran, D., Blei, D., and Airoldi, E. M. (2015). Copula variational inference. In *Advances in Neural Information Processing Systems*, pages 3564–3572.
- Wilson, A. G. and Ghahramani, Z. (2010). Copula processes. In *Advances in Neural Information Processing Systems*, pages 2460–2468.
- Yoshihara, T. (2018). Maximum likelihood estimation of skew-t copulas with its applications to stock returns. *Journal of Statistical Computation and Simulation*, 88(13):2489–2506.
- Yu, X., Nott, D. J., Tran, M.-N., and Klein, N. (2021). Assessment and adjustment of approximate inference algorithms using the law of total variance. *Journal of Computational and Graphical Statistics*, forthcoming.
- Zhang, Z., Nishimura, A., Bastide, P., Ji, X., Payne, R. P., Goulder, P., Lemey, P., and Suchard, M. A. (2021). Large-scale inference of correlation among mixed-type biological traits with phylogenetic multivariate probit models. *The Annals of Applied Statistics*, 15(1):230–251.

Figure 1: Marginals of Different Gaussian Copula Model VAs



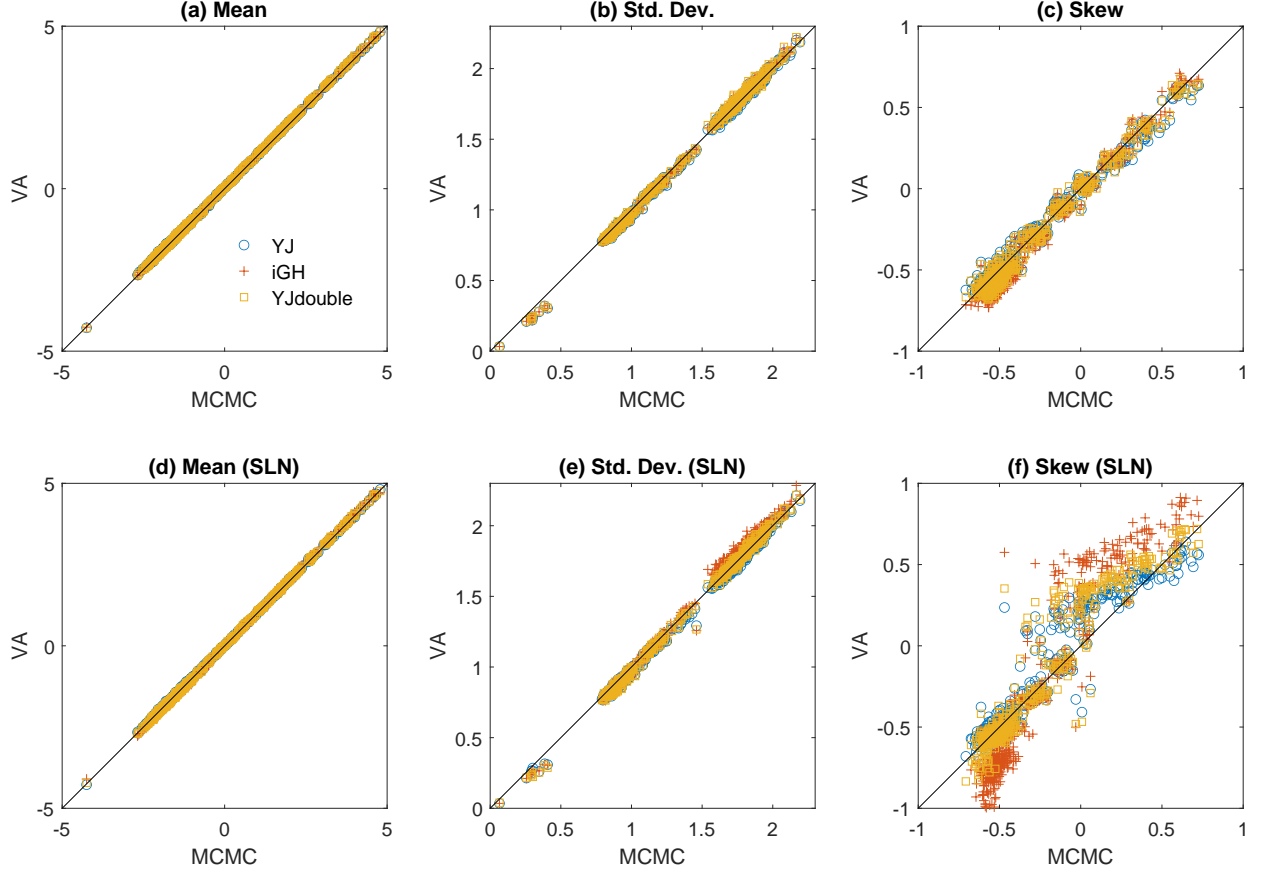
Marginal densities q_i^{SLN2020} (yellow dotted line) and q_{λ_i} at (10) (red dashed line) of optimal VAs to two skew normal (SN) target densities (blue solid line). Both target distributions have the same Pearson skew of 0.8553 and standard deviation $\sigma_{\text{SN}} = 1$. Panel (a) plots VA densities when the target mean is $\mu_{\text{SN}} = 15$, and panel (b) plots VA densities when the target mean is $\mu_{\text{SN}} = 0$. Also reported are the KL divergences for the optimal approximations in parentheses.

Figure 2: Kullback-Leibler Divergence of Gaussian Copula Model VA Marginals



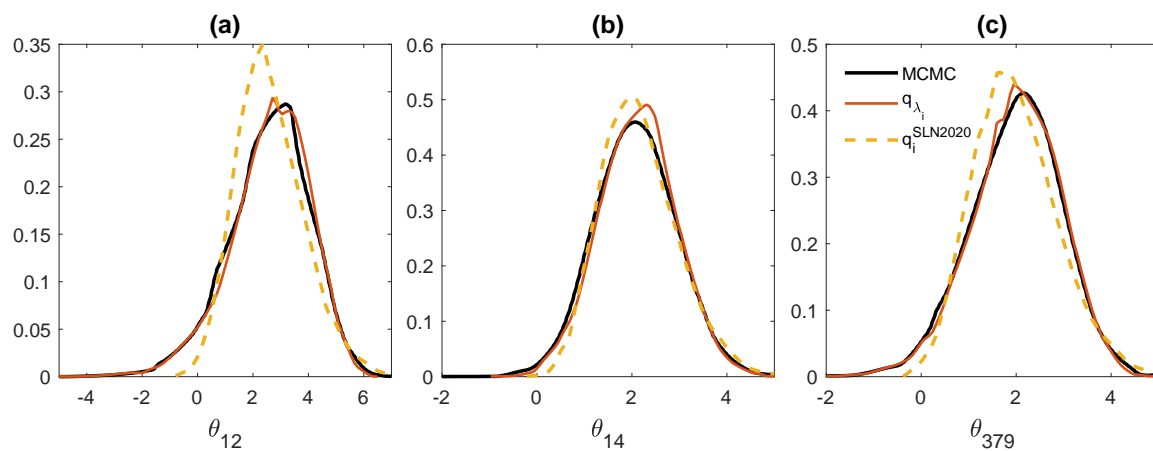
KL divergence of optimal marginal approximations to SN target densities. The SN distributions have a Pearson skew of 0.8553, but different means μ_{SN} and standard deviations σ_{SN} . Gaussian approximations have KL divergence of 0.172 for all target densities (black dashed line), and the approximation q_{λ_i} at (10) has KL divergence of 0.009 for all target densities (solid black line). The KL divergence of $q_i^{SLN2020}$ is plotted as curves for four values of σ_{SN} and $0 < \mu_{SN} < 60$. The two cases corresponding to Figure 1(a,b) are indicated with circles.

Figure 3: Accuracy of Posterior Moments for Mixed Logistic Regression Example



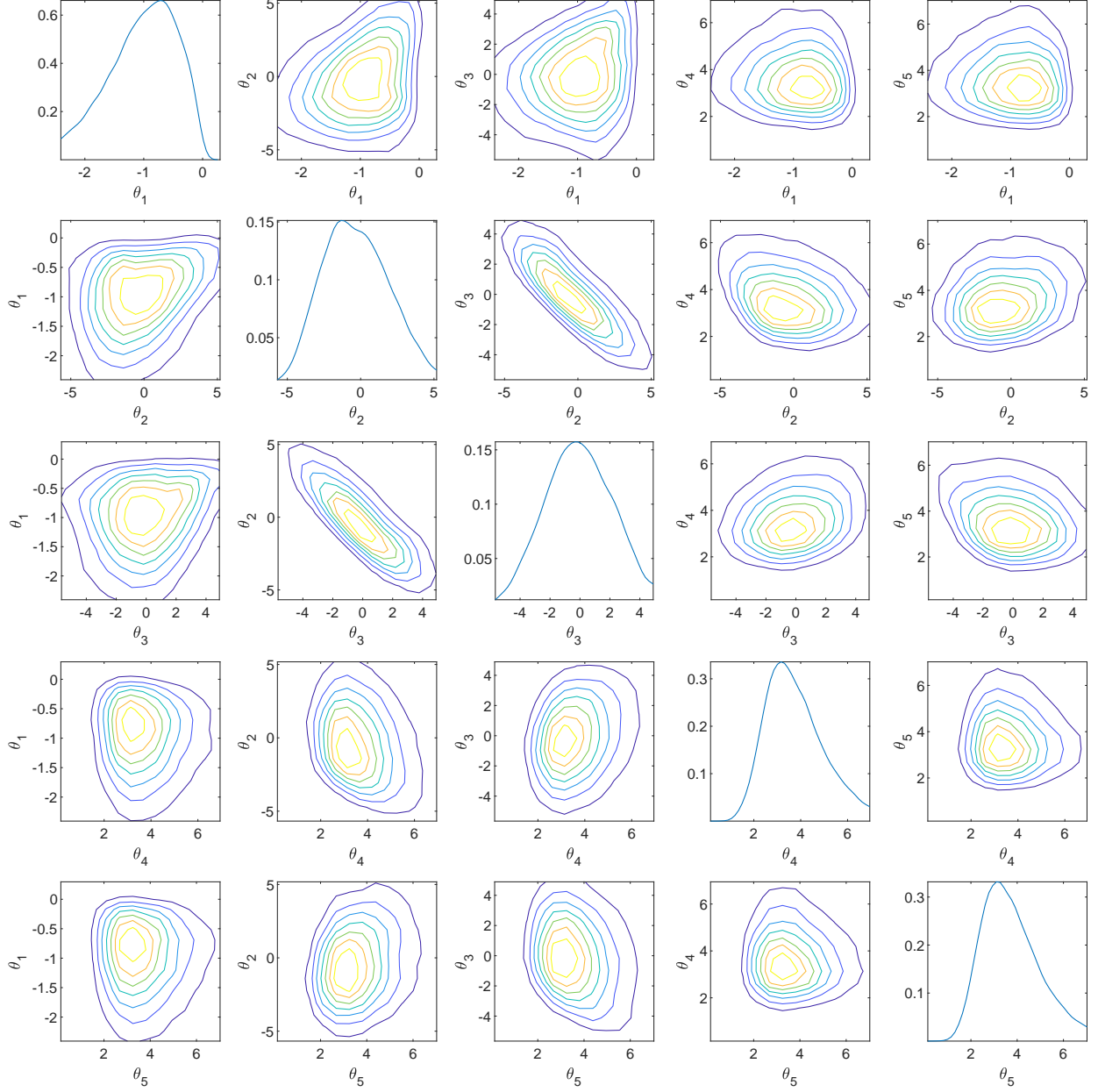
Panels (a)–(c) are for the t-copula model VA proposed here, and panels (d)–(f) are for the Gaussian copula model VA in Smith et al. (2020). In each panel the exact posterior moment (computed using MCMC) is plotted on the horizontal axis, and moment of the VA on the vertical axis. The posterior means, standard deviations and Pearson’s skew are plotted in the first, second and third columns, respectively. In each panel there is a scatter of $m = 509$ points for each of three variational estimators that correspond to the YJ (blue circles), iGH (red cross) and YJ-Double (yellow square) transformations for t_{γ_i} . For panels (a)–(e), the results are very similar for the three transformations, so that most points are close to each other and hard to distinguish.

Figure 4: Posteriors for Three Random Effects in the Mixed Logistic Regression Example



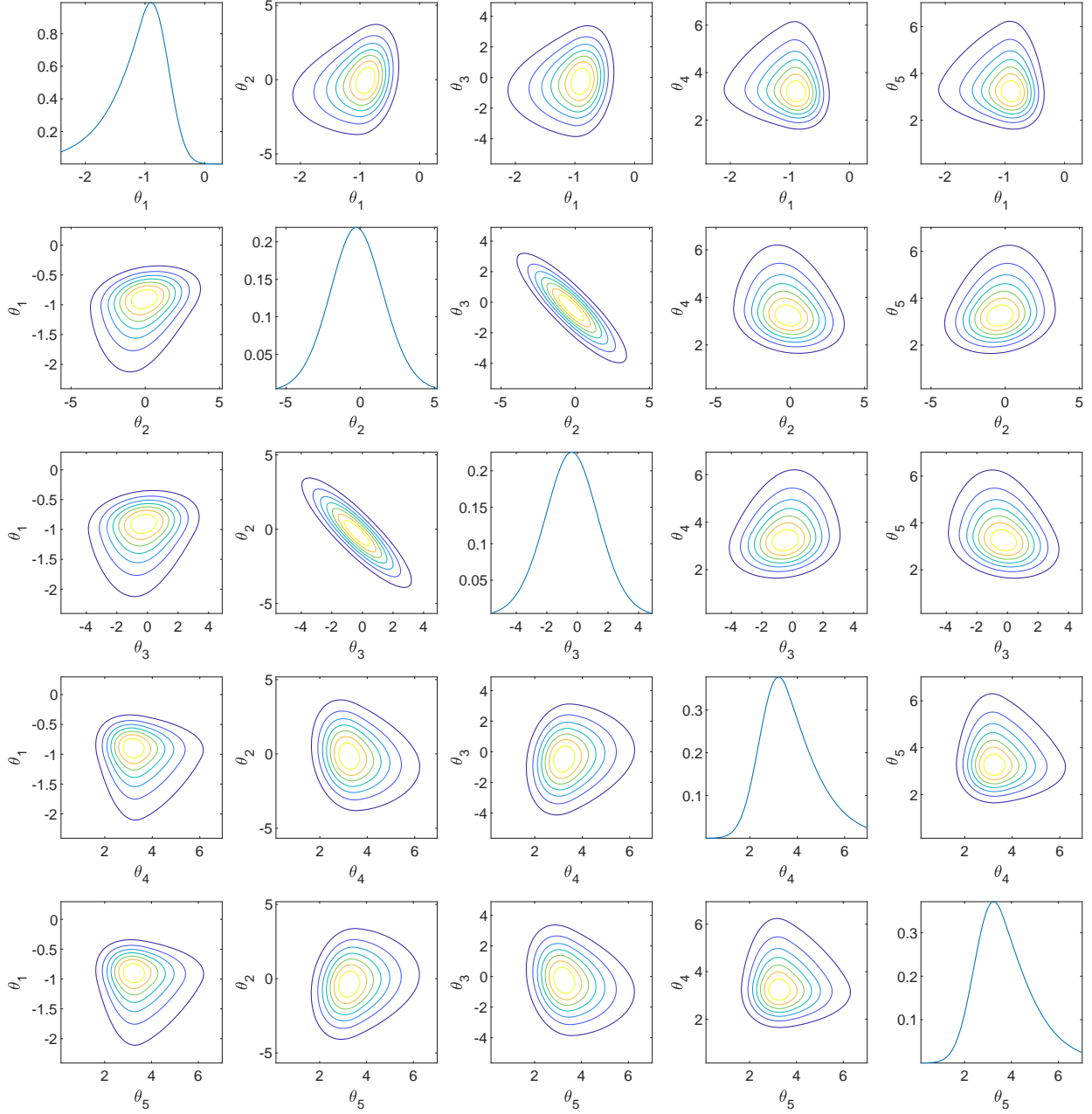
Marginal posterior densities for three random effects. Each panel plots the exact posterior computed by MCMC (black solid thick line), the t-copula model VA q_{λ_i} at (4) (red solid thin line) and that in Smith et al. (2020) q_i^{SLN2020} (yellow dashed line). Both approximations use the iGH transformation.

Figure 5: Exact Posterior for the Two U.S. States Inequality Example



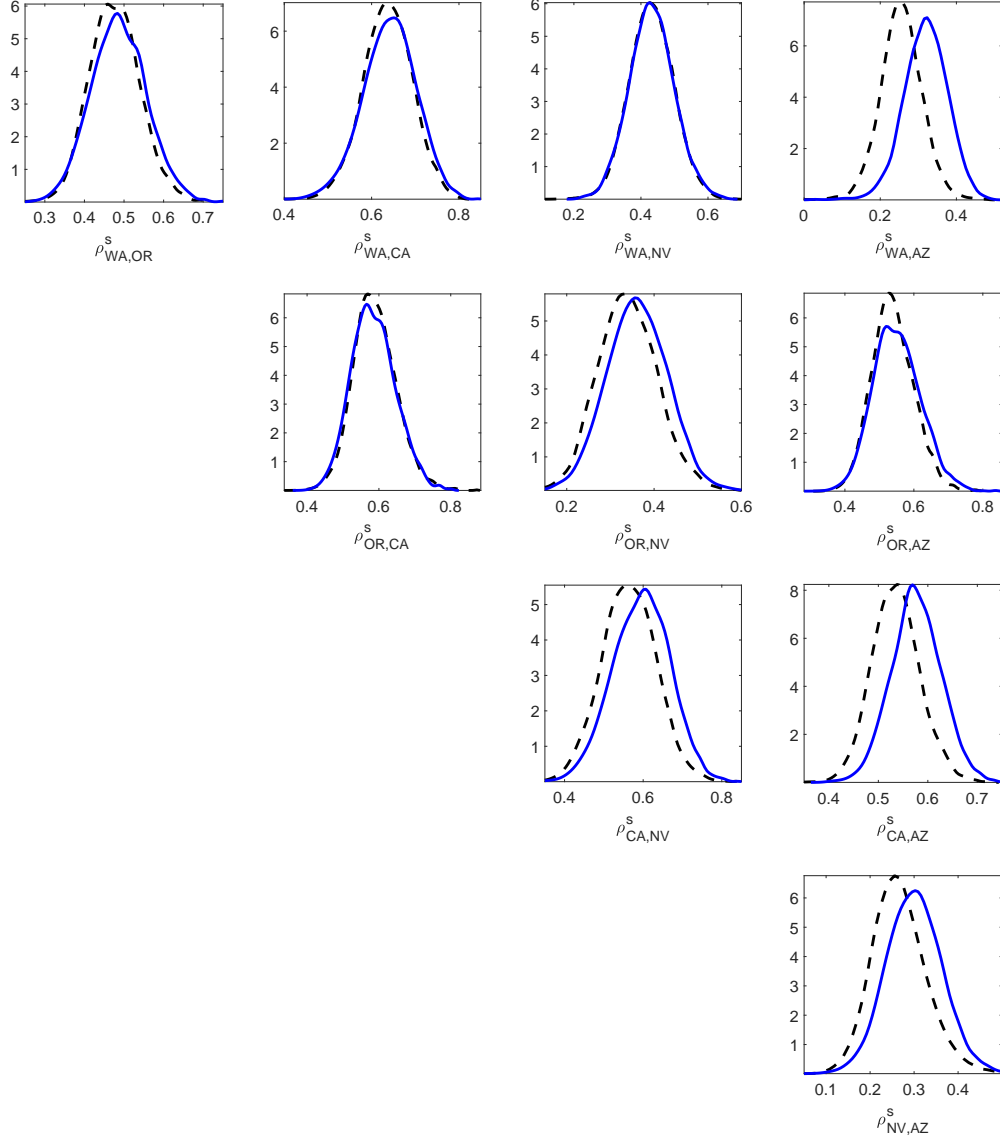
Exact posterior of $(\theta_1, \dots, \theta_5)^\top = (\tau_1, \log \chi_1, \log \nu_1, \log \xi, \log \kappa)^\top$ computed using MCMC. The univariate marginals $p(\theta_i|\mathbf{y})$ are on the leading diagonals, and the bivariate marginals $p(\theta_i, \theta_j|\mathbf{y})$ are on the off-diagonals.

Figure 6: Variational Posterior for the Two U.S. States Inequality Example



Posterior estimates of $(\theta_1, \dots, \theta_5)^\top = (\tau_1, \log \chi_1, \log \nu_1, \log \xi, \log \kappa)^\top$ using the copula model VA with (adjusted) YJ transformations. The marginals $q_{\lambda_i}(\theta_i)$ are on the leading diagonals, and the bivariate marginals—which are bivariate slices of (9)—are on the off-diagonals.

Figure 7: Variational Posterior Densities of Spearman Correlations for Five Western States



Variational posterior densities of the 10 Spearman correlations between the western U.S. states of WA, OR, CA, NV and AZ. The posterior for the more accurate optimal t-copula is the blue solid line, while that from the mean field t-distribution is the black dashed line.

Online Appendix for “Implicit copula variational inference”

This Online Appendix has four parts:

Part A: Notational conventions and matrix differentiation rules used.

Part B: Additional details on derivations in Appendix A.

Part C: Additional details for the regularized correlation matrix model in Section 4.

Part D: Additional empirical results for the U.S. inequality example with 49 states.

Part E: List of MATLAB routines provided.

Part A: Notational conventions and matrix differentiation rules used

We outline the notational conventions that we adopt in computing derivatives throughout the paper, which are the same as adopted in Smith, Loaiza-Maya and Nott (2020). For a d -dimensional vector valued function $g(\mathbf{x})$ of an n -dimensional argument \mathbf{x} , $\frac{\partial g}{\partial \mathbf{x}}$ is the $d \times n$ matrix with element (i, j) $\frac{\partial g_i}{\partial x_j}$. This means for a scalar $g(\mathbf{x})$, $\frac{\partial g}{\partial \mathbf{x}}$ is a row vector. When discussing the SGA algorithm we also sometimes write $\nabla_{\mathbf{x}} g(\mathbf{x}) = \frac{\partial g}{\partial \mathbf{x}}^\top$, which is a column vector. When the function $g(\mathbf{x})$ or the argument \mathbf{x} are matrix valued, then $\frac{\partial g}{\partial \mathbf{x}}$ is taken to mean $\frac{\partial \text{vec}(g(\mathbf{x}))}{\partial \text{vec}(\mathbf{x})}$, where $\text{vec}(A)$ denotes the vectorization of a matrix A obtained by stacking its columns one underneath another. If $g(x)$ and $h(x)$ are matrix valued functions, say $g(x)$ takes values which are $d \times r$ and $h(x)$ takes values which are $r \times n$, then a matrix valued product rule is

$$\frac{\partial g(x)h(x)}{\partial x} = (h(x)^\top \otimes I_d) \frac{\partial g(x)}{\partial x} + (I_n \otimes g(x)) \frac{\partial h(x)}{\partial x}$$

where \otimes denotes the Kronecker product and I_a denotes the $a \times a$ identity matrix for a positive integer a .

Some other useful results used repeatedly throughout the derivations below are

$$\text{vec}(ABC) = (C^\top \otimes A) \text{vec}(B),$$

for conformable matrices A , B and C the derivative

$$\frac{\partial A^{-1}}{\partial A} = -(A^{-T} \otimes A^{-1}).$$

We also write $K_{m,n}$ for the commutation matrix (see, for example, Magnus and Neudecker, 1999).

Last, for scalar function $g(x)$ of scalar-valued argument x , we sometimes write $g'(x) = \frac{d}{dx}g(x)$ and $g''(x) = \frac{d^2}{dx^2}g(x)$ for the first and second derivatives with respect to x whenever it appears clearer to do so.

Part B: Additional details on derivations in Appendix A

Second, we provide further details on the derivation of $\frac{\partial \theta}{\partial \lambda}$. Denote $A = [\mathbf{d} \ B]$ to be the matrix with elements $a_{j,k}$ and $\boldsymbol{\kappa} = (\boldsymbol{\kappa}_1^\top, \dots, \boldsymbol{\kappa}_m^\top)^\top$. We need to compute the derivatives of $\theta = h(\boldsymbol{\varepsilon}, \boldsymbol{\lambda})$ with respect to all the elements in $\boldsymbol{\lambda} = (\boldsymbol{\mu}^\top, \boldsymbol{\sigma}^\top, \boldsymbol{\gamma}^\top, \boldsymbol{\tau}^\top)^\top$:

$$\begin{aligned}\frac{\partial \theta}{\partial \boldsymbol{\mu}} &= I_m \\ \frac{\partial \theta}{\partial \boldsymbol{\sigma}} &= \text{diag}(t_{\gamma_1}^{-1}(\psi_1), \dots, t_{\gamma_m}^{-1}(\psi_m)) \\ \frac{\partial \theta}{\partial \boldsymbol{\gamma}} &= \text{diag}\left(\sigma_1 \frac{\partial t_{\gamma_1}^{-1}(\psi_1)}{\partial \gamma_1}, \dots, \sigma_m \frac{\partial t_{\gamma_m}^{-1}(\psi_m)}{\partial \gamma_m}\right) \\ \frac{\partial \theta}{\partial \boldsymbol{\tau}} &= \frac{\partial \theta}{\partial \psi} \frac{\partial \psi}{\partial \boldsymbol{\kappa}} \frac{\partial \boldsymbol{\kappa}}{\partial \boldsymbol{\tau}} \\ \frac{\partial \theta}{\partial \boldsymbol{\omega}} &= \frac{\partial \theta}{\partial \psi} \frac{\partial \psi}{\partial \boldsymbol{\omega}}\end{aligned}$$

For the last derivative we need to compute the three terms $\frac{\partial \theta}{\partial \psi}$, $\frac{\partial \psi}{\partial \boldsymbol{\kappa}}$, and $\frac{\partial \boldsymbol{\kappa}}{\partial \boldsymbol{\tau}}$. The first term can be computed as

$$\frac{\partial \theta}{\partial \psi} = \text{diag}\left(\sigma_1 \frac{\partial t_{\gamma_1}^{-1}(\psi_1)}{\partial \psi_1}, \dots, \sigma_m \frac{\partial t_{\gamma_m}^{-1}(\psi_m)}{\partial \psi_m}\right).$$

The third term is given as $\frac{\partial \boldsymbol{\kappa}}{\partial \boldsymbol{\tau}} = \text{blockdiag}\left(\frac{\partial \boldsymbol{\kappa}_1}{\partial \boldsymbol{\tau}_1}, \dots, \frac{\partial \boldsymbol{\kappa}_m}{\partial \boldsymbol{\tau}_m}\right)$, with

$$\frac{\partial \boldsymbol{\kappa}_j}{\partial \boldsymbol{\tau}_j} = \text{diag}(\phi(\tau_{j,1})\pi, \dots, \phi(\tau_{j,K-1})\pi, \phi(\tau_{j,K})2\pi).$$

For the second term we know that:

$$\frac{\partial \psi}{\partial \boldsymbol{\kappa}} = \sqrt{w} \left[(\mathbf{z}^\top \otimes I_m) \frac{\partial B}{\partial \boldsymbol{\kappa}} + \text{diag}(\boldsymbol{\epsilon}) \frac{\partial \mathbf{d}}{\partial \boldsymbol{\kappa}} \right] \quad (14)$$

with

$$\frac{\partial B}{\partial \boldsymbol{\kappa}} = \frac{\partial B}{\partial A^\top} \frac{\partial A^\top}{\partial \boldsymbol{\kappa}}$$

and

$$\frac{\partial \mathbf{d}}{\partial \boldsymbol{\kappa}} = \frac{\partial \mathbf{d}}{\partial A^\top} \frac{\partial A^\top}{\partial \boldsymbol{\kappa}}$$

We can write $B = AP_1$ and $\mathbf{d} = AP_2$ where $P_1 = [\mathbf{0}_{K \times 1} \ I_K]^\top$ and $P_2 = (1, \mathbf{0}_{1 \times K})^\top$. Then $\frac{\partial B}{\partial A^\top}$ can be easily computed after noting that

$$\text{vec}(B) = (P_1^\top \otimes I_m) \text{vec}(A) = (P_1^\top \otimes I_m) K_{K+1,m} \text{vec}(A^\top)$$

where $K_{K+1,m}$ denotes a commutation matrix. Then

$$\frac{\partial B}{\partial A^\top} = \left(P_1^\top \otimes I_m \right) K_{K+1,m}.$$

The term $\frac{\partial \mathbf{d}}{\partial A^\top}$ can be computed by noting that

$$\text{vec}(\mathbf{d}) = \left(P_2^\top \otimes I_m \right) \text{vec}(A) = \left(P_2^\top \otimes I_m \right) K_{K+1,m} \text{vec}(A^\top)$$

so that

$$\frac{\partial \mathbf{d}}{\partial A^\top} = \left(P_2^\top \otimes I_m \right) K_{K+1,m}.$$

The elements of the derivative $\frac{\partial A^\top}{\partial \boldsymbol{\chi}} = \text{blockdiag} \left(\frac{\partial \mathbf{a}_1}{\partial \boldsymbol{\chi}_1}, \dots, \frac{\partial \mathbf{a}_m}{\partial \boldsymbol{\chi}_m} \right)$ can be computed as

$$\left\{ \frac{\partial \mathbf{a}_i}{\partial \boldsymbol{\chi}_i} \right\}_{j,l} = \begin{cases} \cos(\boldsymbol{\chi}_{i,j}) \cos(\boldsymbol{\chi}_{i,l}) \prod_{s \in \{1, \dots, j-1\} \setminus l} \sin(\boldsymbol{\chi}_{i,s}) & \text{If } l < j \text{ and } j < K+1 \\ - \prod_{s=1}^j \sin(\boldsymbol{\chi}_{i,s}) & \text{If } l = j \text{ and } j < K+1 \\ \cos(\boldsymbol{\chi}_{i,l}) \prod_{s \in \{1, \dots, j-1\} \setminus l} \sin(\boldsymbol{\chi}_{i,s}) & \text{If } l < j \text{ and } j = K+1 \\ 0 & \text{Otherwise} \end{cases}$$

Replacing all the terms above into (14) we can show that

$$\frac{\partial \psi}{\partial \boldsymbol{\chi}} = \sqrt{w} \left[(\mathbf{z}^\top P_1^\top) \otimes I_m + \text{diag}(\boldsymbol{\epsilon}) \left(P_2^\top \otimes I_m \right) \right] K_{K+1,m} \frac{\partial A^\top}{\partial \boldsymbol{\chi}}.$$

Part C: Additional details for the regularized correlation matrix model in Section 4

This appendix provides further details on the priors and the required gradients and derivatives for the SGA algorithm.

Priors

The priors for all the parameters in the model are

$$\tau_s \sim N(0, 1), \quad \chi_s | \nu_s \sim \mathcal{G}^{-1} \left(\frac{1}{2}, \frac{1}{\nu_s} \right), \quad \xi | \kappa \sim \mathcal{G}^{-1} \left(\frac{1}{2}, \frac{1}{\kappa} \right)$$

$$\nu_1, \dots, \nu_{r(r-1)/2}, \kappa \sim \mathcal{G}^{-1} \left(\frac{1}{2}, 20 \right).$$

To conduct variational inference we transform all parameters to the real line as follows:

- (i) χ_s is transformed to $\tilde{\chi}_s = \log \chi_s$;
- (ii) ξ is transformed to $\tilde{\xi} = \log \xi$;
- (iii) ν_s is transformed to $\tilde{\nu}_s = \log \nu_s$;
- (iv) κ is transformed to $\tilde{\kappa} = \log \kappa$.

After the transformations we obtain the following prior density functions (using the Jacobians of the change of variables)

- (i) $p(\tau_s) = \phi_1(\tau_s; 0, 1)$;
- (ii) $p(\tilde{\chi}_s | \nu_s) \propto \left(\frac{1}{\nu_s} \right)^{0.5} \exp \left(-\frac{1}{2} \tilde{\chi}_s - \frac{1}{\nu_s \exp(\tilde{\chi}_s)} \right)$;
- (iii) $p(\tilde{\xi} | \kappa) \propto \left(\frac{1}{\kappa} \right)^{0.5} \exp \left(-\frac{1}{2} \tilde{\xi} - \frac{1}{\kappa \exp(\tilde{\xi})} \right)$;
- (iv) $p(\tilde{\nu}_s) \propto \exp \left(-\frac{1}{2} \tilde{\nu}_s - \frac{20}{\exp(\tilde{\nu}_s)} \right)$;
- (v) $p(\tilde{\kappa}) \propto \exp \left(-\frac{1}{2} \tilde{\kappa} - \frac{20}{\exp(\tilde{\kappa})} \right)$.

Log-posterior

$$\log g(\boldsymbol{\theta}) = \log p(\mathbf{y} | \boldsymbol{\theta}) + \log p(\boldsymbol{\theta}) \tag{15}$$

$$\propto -\frac{N}{2} \log |\Omega| - \frac{1}{2} \sum_{i=1}^N \mathbf{x}_i^\top (\Omega^{-1} - I_r) \mathbf{x}_i + \log p(\boldsymbol{\theta}) \tag{16}$$

where the term $\log(\prod_{j=1}^r g_j(y_{i,j}))$ is a constant with respect to $\boldsymbol{\theta}$.

Gradient

The model-specific gradient vector for the parameters of the copula model is:

$$\nabla_{\boldsymbol{\theta}} \log g(\boldsymbol{\theta}) = (\nabla_{\tau} \log g(\boldsymbol{\theta})^\top, \nabla_{\tilde{\chi}} \log g(\boldsymbol{\theta})^\top, \nabla_{\tilde{\xi}} \log g(\boldsymbol{\theta})^\top, \nabla_{\tilde{\nu}} \log g(\boldsymbol{\theta})^\top, \nabla_{\tilde{\kappa}} \log g(\boldsymbol{\theta})^\top)^\top.$$

The different terms in this gradient can be computed as

$$\begin{aligned}
\nabla_{\boldsymbol{\tau}} \log g(\boldsymbol{\theta}) &= \left(\sqrt{\xi} \sqrt{\boldsymbol{\chi}} \right) \circ \frac{\partial \log g(\boldsymbol{\theta})}{\partial \boldsymbol{\eta}}^{\top} - \boldsymbol{\tau} \\
\nabla_{\tilde{\boldsymbol{\chi}}} \log g(\boldsymbol{\theta}) &= \frac{1}{2} \boldsymbol{\tau} \circ \left(\sqrt{\xi} \sqrt{\boldsymbol{\chi}} \right) \circ \frac{\partial \log g(\boldsymbol{\theta})}{\partial \boldsymbol{\eta}}^{\top} + \nabla_{\tilde{\boldsymbol{\chi}}} \log p(\tilde{\boldsymbol{\chi}} | \tilde{\boldsymbol{\nu}}) \\
\nabla_{\tilde{\boldsymbol{\nu}}} \log g(\boldsymbol{\theta}) &= \nabla_{\tilde{\boldsymbol{\nu}}} \log p(\tilde{\boldsymbol{\chi}} | \tilde{\boldsymbol{\nu}}) + \nabla_{\tilde{\boldsymbol{\nu}}} \log p(\tilde{\boldsymbol{\nu}}) \\
\nabla_{\tilde{\xi}} \log g(\boldsymbol{\theta}) &= \frac{1}{2} \frac{\partial \log g(\boldsymbol{\theta})}{\partial \boldsymbol{\eta}} \left(\boldsymbol{\tau} \circ \sqrt{\xi} \sqrt{\boldsymbol{\chi}} \right) - \frac{1}{2} + \frac{1}{\kappa \xi} \\
\nabla_{\tilde{\kappa}} \log g(\boldsymbol{\theta}) &= -\frac{1}{2} + \frac{1}{\kappa \xi} - \frac{1}{2} + \frac{1}{\kappa}
\end{aligned}$$

where $\nabla_{\tilde{\boldsymbol{\chi}}} \log p(\tilde{\boldsymbol{\chi}} | \tilde{\boldsymbol{\nu}}) = \left(-\frac{1}{2} + \frac{1}{\nu_1 \chi_1}, \dots, -\frac{1}{2} + \frac{1}{\nu_{r(r-1)/2} \chi_{r(r-1)/2}} \right)^{\top}$,
 $\nabla_{\tilde{\boldsymbol{\nu}}} \log p(\tilde{\boldsymbol{\chi}} | \tilde{\boldsymbol{\nu}}) = \left(-\frac{1}{2} + \frac{1}{\nu_s \chi_s}, \dots, -\frac{1}{2} + \frac{1}{\nu_{r(r-1)/2} \chi_{r(r-1)/2}} \right)^{\top}$, $\nabla_{\tilde{\boldsymbol{\nu}}} \log p(\tilde{\boldsymbol{\nu}}) = \left(-\frac{1}{2} + \frac{1}{\nu_{r(r-1)/2}}, \dots, -\frac{1}{2} + \frac{1}{\nu_{r(r-1)/2}} \right)^{\top}$.

$$\frac{\partial \log g(\boldsymbol{\theta})}{\partial \boldsymbol{\eta}} = \left[-\frac{N}{2} \text{vec}(\Omega^{-1})^{\top} \frac{\partial \Omega}{\partial L} - \frac{1}{2} \left(\sum_{i=1}^N \mathbf{x}_i^{\top} \otimes \mathbf{x}_i^{\top} \right) \frac{\partial \Omega^{-1}}{\partial \Omega} \frac{\partial \Omega}{\partial L} \right] \frac{\partial L}{\partial \boldsymbol{\vartheta}} \frac{\partial \boldsymbol{\vartheta}}{\partial \boldsymbol{\eta}}$$

$$\frac{\partial \Omega}{\partial L} = (I_{r^2} + K_{r,r}) (L \otimes I_r)$$

$$\frac{\partial \Omega^{-1}}{\partial \Omega} = -\Omega^{-1} \otimes \Omega^{-1}$$

$$\frac{\partial \boldsymbol{\vartheta}}{\partial \boldsymbol{\eta}} = \text{blockdiag} \left(\frac{\partial \boldsymbol{\vartheta}_2}{\partial \boldsymbol{\eta}_2}, \dots, \frac{\partial \boldsymbol{\vartheta}_r}{\partial \boldsymbol{\eta}_r} \right)$$

$$\frac{\partial \boldsymbol{\vartheta}_i}{\partial \boldsymbol{\eta}_i} = \text{diag} \left[\phi(\eta_{i,1})\pi, \dots, \phi \left(\eta_{i,i-1} + \Phi^{-1} \left(\frac{1}{4} \right) \right) 2\pi \right]$$

Finally, $\frac{\partial L}{\partial \boldsymbol{\vartheta}}$ is a matrix with elements $\left\{ \frac{\partial L}{\partial \boldsymbol{\vartheta}} \right\}_{(j-1)r+i, (i-1)(r-1)+k} = \frac{\partial l_{i,j}}{\partial \vartheta_{i,k}}$, where

$$\frac{\partial l_{i,j}}{\partial \vartheta_{i,k}} = \begin{cases} \cos(\vartheta_{i,i-1}) \prod_{s=1}^{i-2} \sin(\vartheta_{i,s}) & \text{If } i > 1 \text{ and } j = i \text{ and } k = i-1 \\ \sin(\vartheta_{i,i-1}) \frac{\cos(\vartheta_{i,k})}{\sin(\vartheta_{i,k})} \prod_{s=1}^{i-2} \sin(\vartheta_{i,s}) & \text{If } i > 1 \text{ and } j = i \text{ and } k < i-1 \\ -\prod_{s=1}^j \sin(\vartheta_{i,s}) & \text{If } i > 1 \text{ and } j < i \text{ and } k = j \\ \cos(\vartheta_{i,j}) \frac{\cos(\vartheta_{i,k})}{\sin(\vartheta_{i,k})} \prod_{s=1}^{j-1} \sin(\vartheta_{i,s}) & \text{If } i > 1 \text{ and } j < i \text{ and } k < j \\ 0 & \text{otherwise.} \end{cases}$$

If not specified, all remaining elements of $\frac{\partial L}{\partial \boldsymbol{\vartheta}}$ are zero.

Part D: Additional empirical results for the U.S. inequality example with 49 states

Here we include some additional empirical results for the U.S. income inequality example. Figure A1 provides the kernel density estimates of the marginal densities g_j for the nine most popular U.S. states. These are far from Gaussian, so that a Gaussian copula model that accounts for this is more appropriate than fitting a multivariate normal distribution. The KDE's for the remaining 40 states (unreported) are also far from Gaussian.

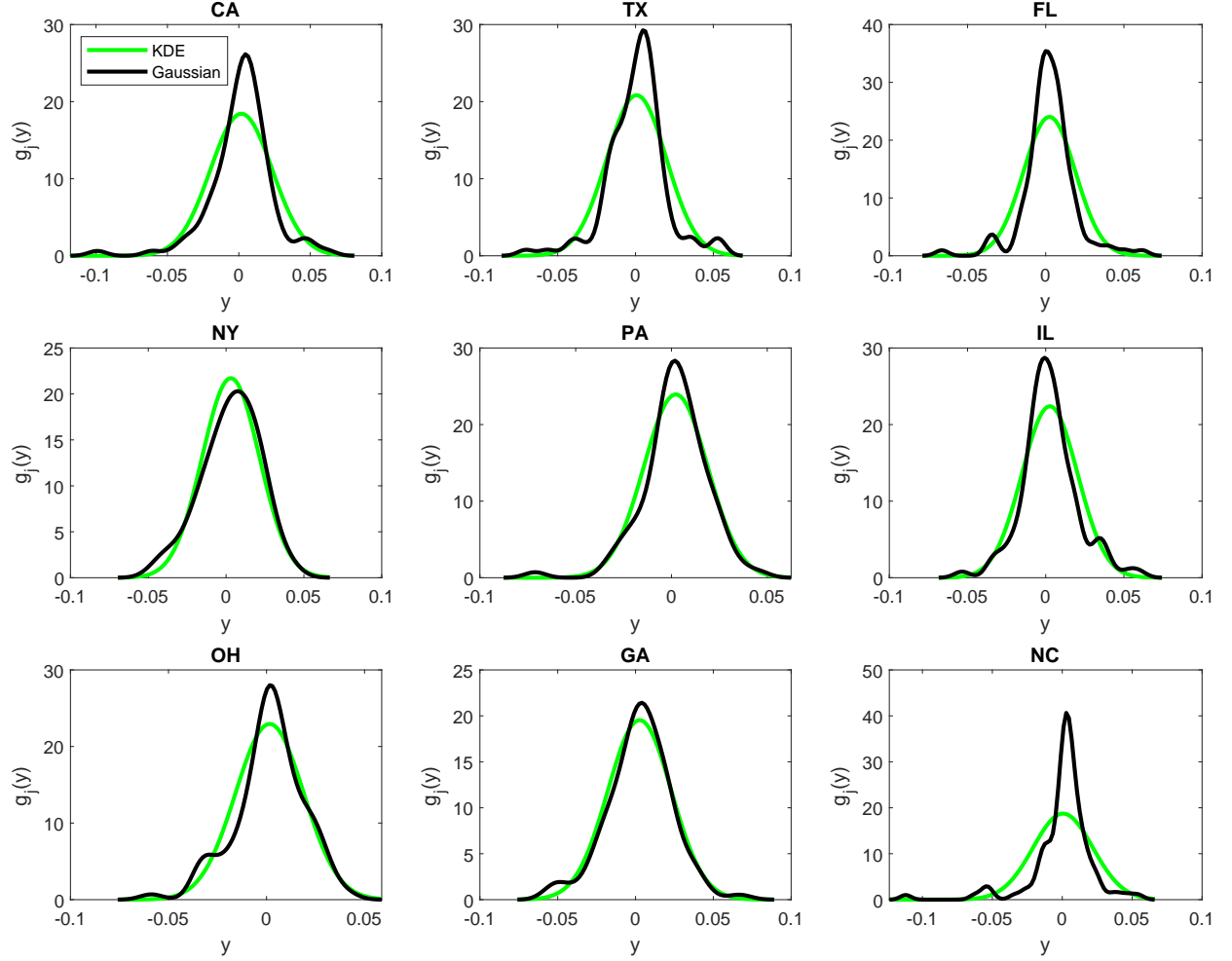
Figure A2 reports the posterior mean estimates of Spearman correlation matrix Ω^s for all 49 U.S. states in our data. These estimates were obtained by simulating draws from $q_{\lambda^*}(\boldsymbol{\theta})$, evaluating the resulting draws of Ω^s and computing their mean. There are no negative Spearman correlations, and the highest dependencies tend to be between geographically adjacent or close states. For example, IL is positively dependent with NY, PA and MA.

Figure A3 plots the approximate ELBO values against step number for the twenty VAs in Table 2 of the manuscript. The lower bound value is approximate because in the SGA algorithm with the re-parameterization gradient, at each step we have a single draw from f_ε and evaluate

$$\begin{aligned}\mathcal{L}(q_\lambda) &= E_{f_\varepsilon} [\log g(h(\varepsilon, \boldsymbol{\lambda})) - \log q_\lambda(h(\varepsilon, \boldsymbol{\lambda}))] \\ &\approx \log g(h(\varepsilon, \boldsymbol{\lambda})) - \log q_\lambda(h(\varepsilon, \boldsymbol{\lambda})), \text{ for } \varepsilon \sim f_\varepsilon\end{aligned}$$

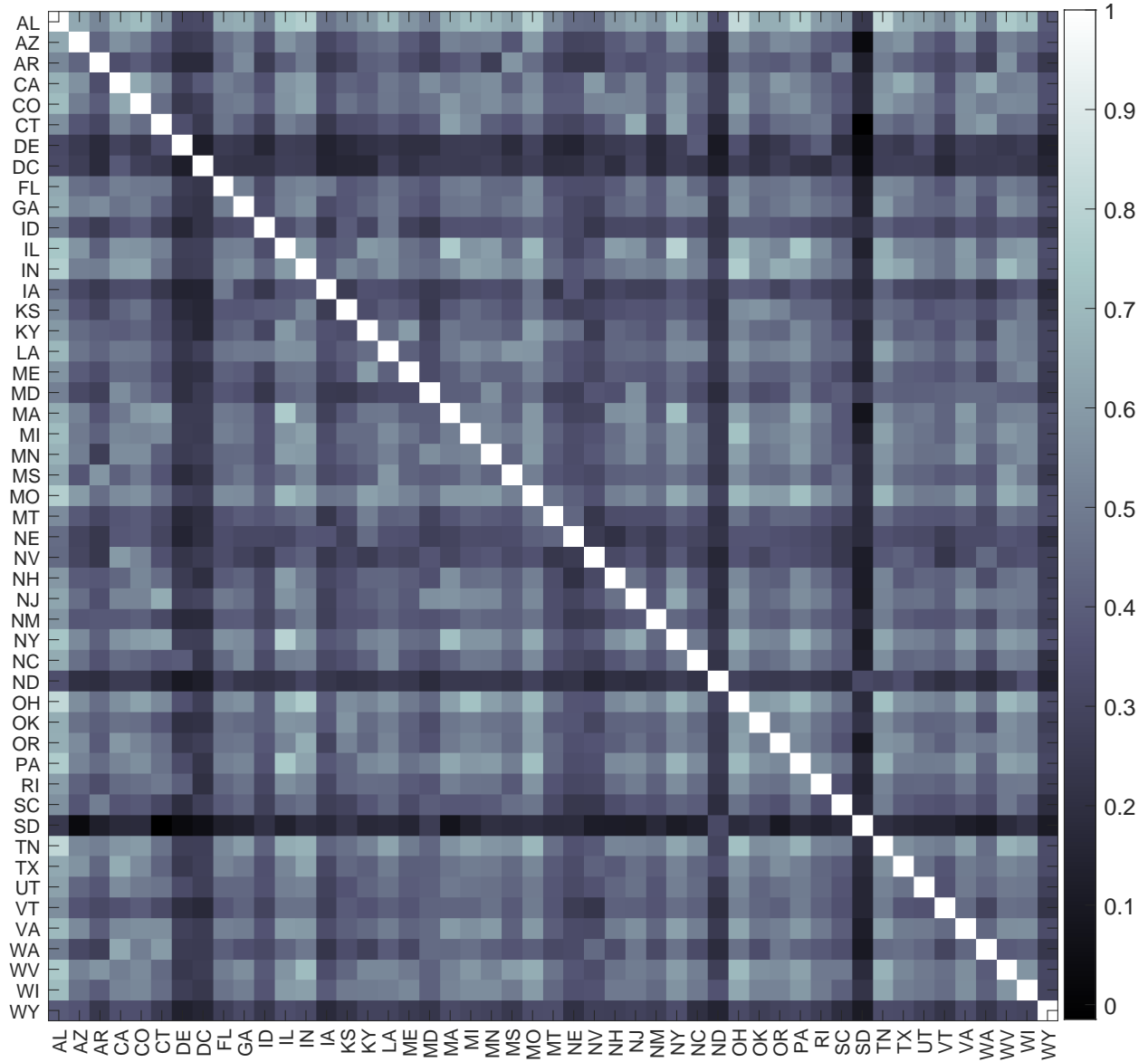
This makes the trace plots noisy, which is also the case for those produced in Ong, Nott and Smith (2018), and Smith, Loaiza-Maya and Nott (2020). Generating multiple draws from f_ε and averaging produces a less noisy approximation of the ELBO function, but slows the SGA algorithm dramatically and is typically not done when using the re-parameterization gradient. This is also why we report the median ELBO values over the last 500 steps (i.e. $\overline{\text{LB}}$) in Table 2. Notice that the SGA algorithm appears to converge by this metric in around 5000 - 10,000 steps for all 20 VAs considered. Each panel gives the trace for a different VA, and the arrangement of the panels matches that of the reported values of $\overline{\text{LB}}$ in Table 2 of the manuscript.

Figure A1: Marginal Data Density Estimates for Nine Most Populous U.S. States



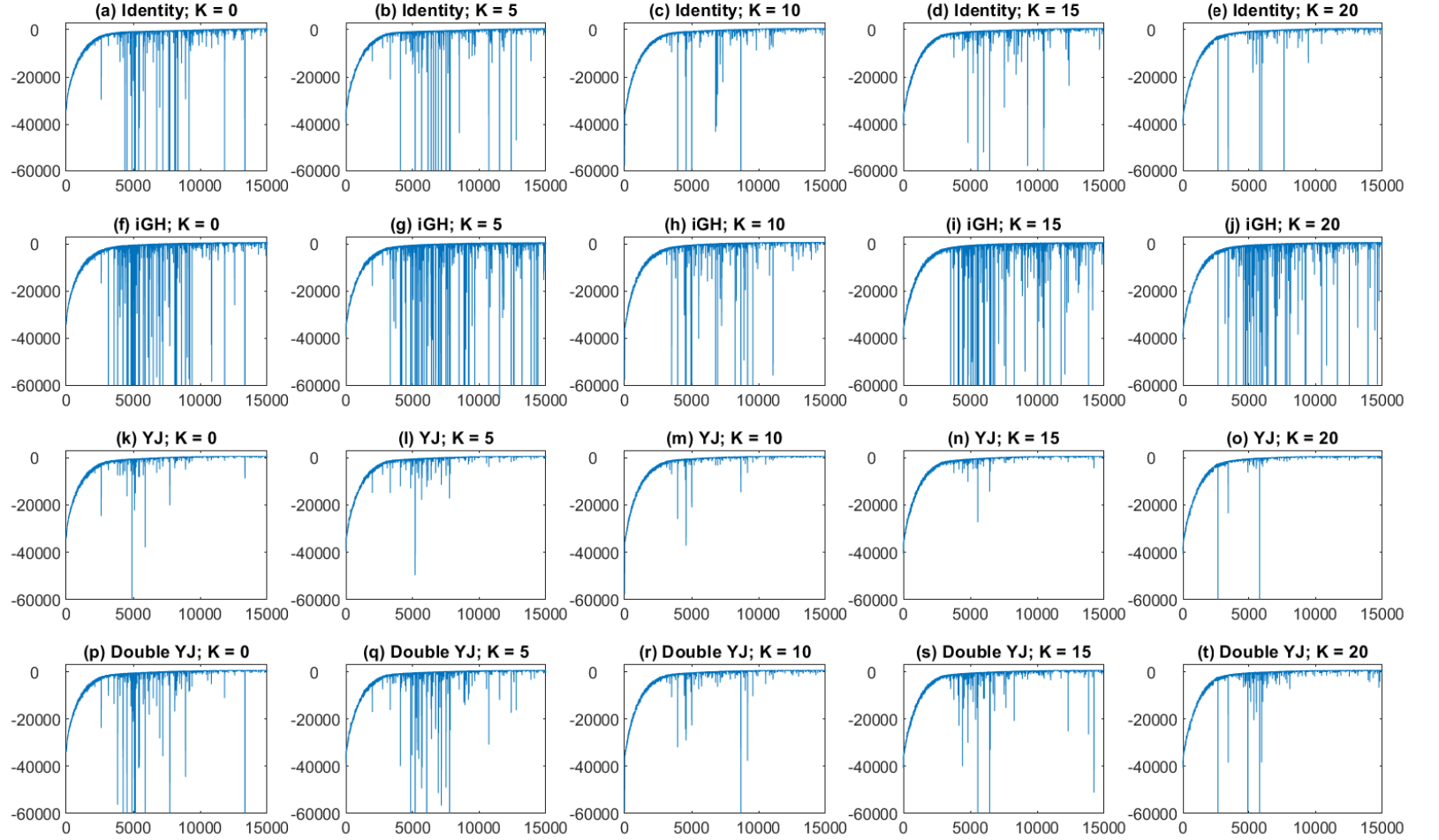
Marginal density estimates of $g_j(y) = \frac{d}{dy}G_j(y)$ for the nine most populous U.S. states. In each panel the KDE (black line) is used to compute the copula data $u_{t,j} = G_j(y_{t,j})$, while the fitted Gaussian (green line) is plotted for comparison.

Figure A2: Variational Posterior Mean of Spearman Correlations in U.S. Inequality Example



Posterior mean estimates of Spearman correlation matrix Ω^s for all 49 U.S. states in our data. These estimates were obtained by simulating draws from $q_{\lambda^*}(\boldsymbol{\theta})$, evaluating the resulting draws of Ω^s and computing their mean.

Figure A3: Evidence Lower Bound for VAs in U.S. Inequality Example



Rows correspond to different transformations and columns correspond to different number of factors in factor covariance structure.

Part E: List of MATLAB routines provided

As part of the Supplementary Material, we provide the MATLAB code and data employed in this study. Details on how to replicate our results using this code are given in README files. Below we also provide a list of the main MATLAB routines employed. Note that these can be used to implement our method with other statistical models.

1. High level functions used to implement our variational inference approach include:
 - VB_step**: updates the variational parameter according to $\boldsymbol{\lambda}^{(s+1)} = \boldsymbol{\lambda}^{(s)} + \boldsymbol{\delta}^{(s)} \circ \widehat{\nabla_{\lambda} \mathcal{L}(q_{\lambda})}$, for the Gaussian copula VA
 - VB_step_tcop**: updates the variational parameter according to $\boldsymbol{\lambda}^{(s+1)} = \boldsymbol{\lambda}^{(s)} + \boldsymbol{\delta}^{(s)} \circ \widehat{\nabla_{\lambda} \mathcal{L}(q_{\lambda})}$, for the t-copula VA
 - VBtransf.m**: Implements variational inference using the proposed copula approximation
2. Functions used to evaluate the re-parameterization gradient efficiently:
 - dxT_dkappa**: compute term $\frac{\partial A^{\top}}{\partial \boldsymbol{\kappa}}$
 - dBd_dkappa.m**: compute the terms $\frac{\partial B}{\partial \boldsymbol{\kappa}}$ and $\frac{\partial d}{\partial \boldsymbol{\kappa}}$
 - dthetadkappa.m**: compute the term $\frac{\partial \boldsymbol{\theta}}{\partial \boldsymbol{\kappa}} = \frac{\partial \boldsymbol{\theta}}{\partial \boldsymbol{\psi}} \frac{\partial \boldsymbol{\psi}}{\partial \boldsymbol{\kappa}}$
 - dkappa_dtkappa.m**: compute the term $\frac{\partial \boldsymbol{\kappa}}{\partial \boldsymbol{\tau}}$
 - dwdnu.m**: compute expression $\frac{\partial}{\partial \nu} F_W^{-1}(u; \nu)$ where F_W is the t-distribution cdf
 - dphidnu.m**: compute the term $\frac{\partial \boldsymbol{\psi}}{\partial \nu}$ for t-copula approximation
 - dthetadnu.m**: compute the term $\frac{\partial \boldsymbol{\theta}}{\partial \nu} = \frac{\partial \boldsymbol{\theta}}{\partial \boldsymbol{\psi}} \frac{\partial \boldsymbol{\psi}}{\partial \nu}$ for t-copula approximation
 - dtheta_dtau**: compute the term $\frac{\partial \boldsymbol{\theta}}{\partial \boldsymbol{\gamma}}$
 - grad_theta_logq.m**: compute term $\nabla_{\boldsymbol{\theta}} \log q_{\lambda}(\boldsymbol{\theta})$ for the Gaussian copula VA
 - grad_theta_logq_tcop.m**: compute term $\nabla_{\boldsymbol{\theta}} \log q_{\lambda}(\boldsymbol{\theta})$ for the t-copula VA
 - gradient_compute.m**: compute $\widehat{\nabla_{\lambda} \mathcal{L}(q_{\lambda})} = \frac{dh(\boldsymbol{\varepsilon}, \boldsymbol{\lambda})}{d\boldsymbol{\lambda}}^{\top} (\nabla_{\boldsymbol{\theta}} \log g(\boldsymbol{\theta}) - \nabla_{\boldsymbol{\theta}} \log q_{\lambda}(\boldsymbol{\theta}))$ for the Gaussian copula VA
 - gradient_compute_tcop.m**: compute $\widehat{\nabla_{\lambda} \mathcal{L}(q_{\lambda})} = \frac{dh(\boldsymbol{\varepsilon}, \boldsymbol{\lambda})}{d\boldsymbol{\lambda}}^{\top} (\nabla_{\boldsymbol{\theta}} \log g(\boldsymbol{\theta}) - \nabla_{\boldsymbol{\theta}} \log q_{\lambda}(\boldsymbol{\theta}))$ for the t-copula VA
3. Low-level functions associated with the iGH and YJ transformations:
 - gh.m**: compute the G&H transformation
 - igh.m**: compute the inverse G&H transformation
 - dgh_g.m dgh_h.m**: compute the derivatives of the G&H transformation with respect to g and h , respectively
 - dgh.m**: compute the first derivative of the G&H transformation with respect to its argument
 - dgih.m**: compute the first derivative of the inverse G&H transformation with respect to its argument
 - ddgh.m**: compute the second derivative of the G&H transformation with respect to its argument
 - ddigh.m**: compute the second derivative of the inverse G&H transformation with respect to its argument

YJ.m: compute the YJ transformation

iYJ.m: compute the inverse YJ transformation

diYJ_deta.m: compute the derivatives of the YJ transformation with respect to γ parameter

dYJ.m: compute the first derivative of the YJ transformation with respect to its argument

diYJ.m: compute the first derivative of the inverse YJ transformation with respect to its argument

ddYJ.m: compute the second derivative of the YJ transformation with respect to its argument